The DOI for this manuscript is

DOI:10.2151/jmsj.2021-037

J-STAGE Advance published date: March 12th, 2021

Hybrid Assimilation of Satellite Rainfall Product with High Density Gauge Network to Improve Daily Estimation: a case of Karnataka, India

Prashant KUMAR, R. M. GAIROLA

Atmospheric and Oceanic Sciences Group, EPSA,

Space Applications Centre, ISRO, India

Takuji KUBOTA

Earth Observation Research Center,

Japan Aerospace Exploration Agency, Japan

and

C. M. KISHTAWAL

Atmospheric and Oceanic Sciences Group, EPSA,

Space Applications Centre, ISRO, India

February 24, 2020

Corresponding author: Prashant Kumar, Atmospheric and Oceanic Sciences Group, EPSA, Space Applications Centre, ISRO, India.

Email: kam3545@gmail.com

Tel: +91-9375785190

Abstract

Accurate rainfall estimation during Indian summer monsoon (ISM) is one of the most crucial activities in and around the Indian Sub-continent. Japan Aerospace Exploration Agency (JAXA) provides a couple of Global Satellite Mapping of Precipitation (GSMaP) rainfall products viz. the GSMaP_MVK, which is a satellite based product calculated with ancillary data including global objective analysis data, and the GSMaP_Gauge, which is adjusted by global rain gauges. In this study, the daily rainfall amount from the GSMaP rainfall product (version 7) is validated against a dense rain gauge network over Karnataka, one of southwestern states of India, during ISM 2016—2018. Further, as the primary objective, these dense rain gauge observations are assimilated in the GSMaP rainfall product using hybrid assimilation method to improve the final rainfall estimate. The hybrid assimilation method is a combination of two-dimensional variational (2D-Var) method and Kalman filter, in which 2D-Var method is used to merge rain gauge observations and Kalman filter is used to update background error in the 2D-Var method. Preliminary verification results suggest that GSMaP_Gauge rainfall has sufficient skill over north interior Karnataka (NIK) and south interior Karnataka (SIK) regions, with large errors over the orographic heavy rainfall region of the Western Ghats. These errors are larger in the GSMaP_MVK rainfall product over orographic heavy rainfall regions. Hybrid assimilation results of randomly selected rain gauge observations improve the skill of GSMaP_Gauge and GSMaP_MVK rainfall products, when compared with independent rain gauges observations. These improvements in daily rainfall are more prominent over orographic heavy rainfall regions. GSMaP_MVK rainfall product shows larger

improvement due to absence of the gauge adjustment in the JAXA operational processing. The superiority of hybrid assimilation method against Cressman and optimal interpolation methods for impacts of utilized rain gauge numbers are also presented in this study.

Keywords: GSMaP rainfall; Karnataka State Natural Disaster Monitoring Centre rain gauge network; Two-dimensional variational method; Orography, Kalman Filter.

1. Introduction

Reliable rainfall estimation is vital for Indian agriculture industry mainly during the Indian summer monsoon (ISM) season that has a large socio-economic impact (Turner et al. 2019). Accurate rainfall estimates are also important for weather forecasting applications, prediction of water-related natural hazards such as floods, droughts, landslides, etc. (Kumar et al. 2014; Chen et al. 2015). Despite the fact that rainfall is one of the most crucial parameters for various applications, availability of accurate and reliable rainfall data on finer spatial and temporal scales is still a challenge (Wang, W. et al. 2017; Wang, Z. et al. 2017; Anjum et al. 2018). Furthermore, rainfall is highly varying in space and time-scale, and its estimation is complex both with ground observations (rain gauges and weather radar) and with satellite data. The sparse distribution of rain gauges and weather radars mainly in mountainous and deeper oceanic regions limits various applications on global and regional scale. On the other hand, space-borne sensors provide homogeneous spatial and temporal distribution of rainfall (Gairola et al. 2015). However, the accuracy of satellite-retrieved rainfall should be assessed with ground observations due to inherent limitations of retrieval algorithms (Chiaravalloti et al. 2018). As space-borne sensors provide instantaneous global scanning of rainfall and rain gauges give accurate but point measurements of rainfall, the verification of satellite-retrieved rainfall against ground observations itself is a major challenge. The problem is even more stimulating under complex topographic conditions, dense vegetation areas and coastal regions (e.g., Brocca et al. 2014; Maggioni et al. 2016; Chiaravalloti et al. 2018). Another major problem for the accurate rainfall estimation is merging ground observations with satellite-estimates of rainfall.

Sun et al. (2018) presented the comprehensive review of the 30 global rainfall datasets (viz. gauge-based GPCC (Global Precipitation Climatology Centre), CPC (Climate Prediction Center), satellite-retrieved Global Satellite Mapping of Precipitation

(GSMaP), TRMM (Tropical Rainfall Measuring Mission), and reported large differences over complex mountain regions including tropics. Authors also pointed out the issues of the number and spatial coverage of the gauge observations, rainfall retrieval algorithms and data assimilation procedures to generate realistic rainfall reanalysis and merge-rainfall product. Kubota et al. (2009) also compared six satellite derived rainfall products including Japan Aerospace Exploration Agency (JAXA) GSMaP rainfall against ground radar dataset calibrated by rain gauges around Japan. Authors found best validation results over the ocean, and reported relatively poor results over mountain regions. Shige et al. (2013) demonstrated that the GSMaP estimates in a case shown by Kubota et al. (2009) could be improved by utilization of more representative profiles in the orographic rainfall. Further, Taniguchi et al. (2013) modified GSMaP rainfall product using an orographic/non-orographic rainfall classification scheme based upon orographically forced upward motion and moisture flux convergence. Trinh-Tuan et al. (2019) showed a clear dependence of biases in the GSMaP estimates over Central Vietnam on elevation and zonal wind speed, suggesting the need to improve orographic rainfall estimations. Nodzu et al. (2019) also examined the effect of interaction between wind and topography on the GSMaP performance over northern Vietnam and suggested that consideration of the orographic effects with wind information may further improve the accuracy of rainfall.

Various studies are performed to evaluate the quality of satellite-retrieved rainfall against rain gauge networks over India (Sharifi et al. 2018; Singh et al. 2019 and references therein). Singh et al. (2019) compared diverse rainfall products against India Meteorological Department (IMD) rain gauges during summer monsoon 2016 and found large differences between satellites derived rainfall products and rain gauges over Karnataka, southwestern India. Prakash et al. (2018) found relatively smaller error in gauge adjusted GSMaP as compared to IMERG (Integrated Multi-satellite Retrievals for Global Precipitation Measurement (GPM)) and TMPA (TRMM multisatellite precipitation analysis) mainly over the regions of low rainfall and the western coast of India. Earlier studies (Palazzi et al. 2013; Hu et al. 2016; Shah and Mishra 2016) also suggested drawbacks of gauge-based estimates and satellite retrievals over mountainous regions, particularly in the Western Ghats mountain range, northeast India, and in the foothills Himalaya. In general, these studies over different parts of the globe and target location of the Western Ghats in southwestern India suggest that the gauge-adjusted rainfall better represents the intrinsic variability of rainfall with more reliability.

The synergy of rain gauge observations with satellite based rainfall estimates in case of gauge-adjusted rainfall estimation are attempted in several previous studies (Gairola and Krishnamurti 1992; Adler et al. 2003; Mitra et al. 2003; Huffman et al. 2007; Roy Bhowmik and Das 2007; Krishnamurti et al. 2009; Gairola et al. 2012). To merge rain gauge observations with INSAT (Indian National SATellite) satellite retrieved rainfall at 1° × 1° spatial resolution, Roy Bhowmik and Das (2007) used an objective analysis method over the Indian landmass for ISM rainfall. Gairola et al. (2015) developed a merged rainfall method by blending rain gauge observations with geostationary Kalpana-1 satellite-derived IMSRA (INSAT retrieved Multi-Spectral Rainfall Algorithm) rainfall estimates using an objective criterion of successive correction method. Authors found considerable improvements in terms of correlation, bias and root-mean-square error after objective analysis, especially over the regions where density of rain gauge was better. Mitra et al. (2009) used a similar approach for blending rain gauge data with the near-real time TMPA rainfall product over India for monsoon rainfall monitoring. The major drawback of the objective analysis techniques is that it does not consider the uncertainties (or errors) in first guess (here satellite rainfall) and observation (here rain gauge) inputs. Thus, the effective merging technique is still required to improve rainfall estimation in terms of both better resolution and accuracy taking into the consideration of errors in both satellite and ground rainfall together.

In this context, the variational method is popularly known for considering inconsistencies (or errors) in input parameters and provides its optimal estimation. The optimal state is achieved by iterative method in variational method and it is less computationally intensive as compared to sequential assimilation methods like optimal interpolation. Earlier, Bianchi et al. (2013) used variational method to combine rain gauge, weather radar and microwave observations with associated uncertainties to retrieve rain rate. Li et al. (2015) implemented variational method to prepare high-resolution hourly rainfall using China Meteorological Administration gauges and CMORPH (Climate Prediction Center Morphing; Joyce et al. 2004) rainfall products. In general, variational method does not consider evolution (or flow) of uncertainties in satellite rainfall (also called as background error), which are considered as a fixed diagonal matrix in earlier studies. These deficiencies in variational method can be resolved to some extent with the implementation of Kalman filter that can simulate the flow of background error. Thus, a hybrid assimilation method, combination of two-dimensional variational (2D-Var) method and flow dependent background error from Kalman filter, is required to prepare gauge-adjusted rainfall product (Cheng et al. 2010; Daley 1997). This hybrid method combines the advantages of excellent spatial coverage from satellite measurement and accurate rainfall estimates from rain gauge data with their uncertainties, and has the potential for optimal combination of rainfall estimation from both the sources simultaneously.

Thus, the objective of this study is to develop a hybrid assimilation method for merge rainfall product over a unique-site that is well represented by sufficient ground observations (around 6502 stations). In this study, first the GSMaP rainfall products are compared with dense rain gauge observations over Karnataka, India during ISM 2016—2018 for evaluating the daily rainfall amount. Around half of the randomly selected rain gauges are merged with GSMaP rainfall products using hybrid assimilation method. These new daily rainfall estimates are verified against the rest of the independent gauges and IMERG final rainfall product. Section 2 discussed the various rainfall data used in this study, followed by results and discussions in section 3. These findings are concluded in section 4.

2. Data Used

2.1. KSNDMC Rain Gauge Network

The Indian state of Karnataka is located within 11°50' N and 18°50' N latitudes and 74° E and 78°50' E longitudes (Fig. 1a). This state is situated on not only a tableland region, but also a coastal plains and mountain slopes in the western part of the Deccan Peninsular region of India (Figs. 1b,d). The dense rain gauge network (6502 stations in 2018 with average rain gauge density of ~6100 stations during years 2016—2018) of the KSNDMC (Karnataka State Natural Disaster Monitoring Centre) is used in this study during ISM 2016—2018 (Fig. 1a). The rain gauge sensor used in this network is a tipping bucket with low tolerance using material of polycarbonate or industrial standard metal. The KSNDMC gauges consist of a funnel that collects and channels precipitation into a small container. Every day at 0830 Indian Standard Time (IST) (0300 UTC (Universal Time Coordinate)), the container tips and empties the collected water and produces a signal in an inbuilt electrical circuit. The tolerance is limited by the precision of the instrument that is 0.5 mm. The precision of the instrument is 1% of rainfall intensity up to 50 mm per day, and 2% of rainfall intensity of 50 to 100 mm day^{-1} (Mohapatra et al. 2017). The original time resolution of the observations is every 15 minutes using a tipping count method (0.2/0.5 mm per tip) with an operating range up to 600 mm hour^{-1}, but in this study, 24 hours (last day 0830 IST to today 0830 IST) accumulated rainfall observations (valid at 0830 IST) are used for verification and assimilation. In this study, Karnataka state is divided into four meteorological zones by state boundaries defined as (1) ***Coastal Karnataka***: a region of heavy rainfall that receives an average June to September (hereafter JJAS) rainfall of 2517 mm, far in excess of rest of state, (2) ***North Interior Karnataka (NIK)***: an arid zone that receives 526 mm of average rainfall in JJAS, (3) ***South Interior Karnataka (SIK)***: This zone receives 518 mm of average rainfall in JJAS, and (4) ***Malnad (Malenadu) Region***: that comprises of Western Ghats, a mountain range inland from the Arabian Sea rising to about 900 meters average height, and with moderate to very high rainfall with 1390 mm of average normal rainfall in JJAS period. These average rainfall amounts for different regions are based on long-term ground based observations (from years 1960—2010) over Karnataka, India. Total 6502 rain gauges available in 2018 are distributed in these four regions viz. coastal (650 gauges), Malnad (901 gauges), NIK (2737 gauges) and SIK (2214 gauges) as shown in Fig. 1a.

Figure 1b shows the map of topography at 30-second spatial resolution from the United State Geological Survey (USGS) available with the Weather Research and Forecasting model (Attada et al. 2018) over the study region. Figure 1c shows mean JJAS rainfall at 0.1-degree spatial resolution from 16-years TRMM/PR data (TRMM-PR (Precipitation Radar) Precipitation System Dataset Version 2.2; Hirose et al. 2009, 2017a,b; Hirose and Okada 2018). Similar to Fig. 1 in Shige et al. (2017), a climatological relationship between topography and rainfall around Karnataka is examined here using the TRMM/PR data. Figure 1d shows cross-shore distribution of rainfall and topography average across the rectangular box selected over the Western Ghats (Fig. 1c). The maximum value of rainfall is obtained mostly over the coastal and windward side of the mountainous regions. Rainfall values are decreased noticeably in the NIK and SIK rain shadow regions that are also represented by the mean TRMM-PR rainfall (Fig. 1c).

2.2 JAXA GSMaP Rainfall

With the notable success of the TRMM, National Aeronautics and Space Administration (NASA) and JAXA have launched the GPM Core Observatory in early 2014 to provide latest generation of satellite-based near real-time precipitation and snowfall estimates (Hou et al. 2014; Skofronick-Jackson et al. 2017). The GSMaP rainfall product has been developed by the JAXA as the Japanese GPM standard product (Kubota et al. 2020). Core algorithms of the GSMaP products are based on those provided by the GSMaP project: passive microwave (PMW) precipitation retrieval algorithm, PMW–IR (InfraRed) combined algorithm and gauge-adjustment algorithm. The GSMaP algorithm consists of the following steps: 1) calculating the rainfall rate from PMW sensors (Kubota et al. 2007; Aonashi et al. 2009; Shige et al. 2009) with ancillary data including global objective analysis data provided by the Japan Meteorological Agency; 2) using Morphing technique to propagate rainfall-affected area; 3) refining the estimated data using Kalman filter approach (Ushio et al. 2009); 4) adjusting rain rates using the National Oceanic and Atmospheric Administration (NOAA) CPC unified gauge-based analysis of global daily rainfall (Mega et al. 2019). The spatial distribution of NOAA/CPC gauges (Chen et al. 2008) over study region are shown in Fig. 1a (as black star). The rainfall retrieval algorithms of JAXA GSMaP have been upgraded further in the GPM-era as described in Kubota et al. (2020). Heavy rainfall associated with shallow orographic rainfall systems was underestimated by the GSMaP algorithms owing to weak ice scattering signatures (Kubota et al. 2009, Shige et al. 2013). Therefore, orographic rainfall estimation method using the global objective analysis data was developed exclusively and installed in the GSMaP PMW algorithm (Shige et al. 2013, 2014; Yamamoto and Shige 2015; Yamamoto et al. 2017).

The GSMaP rainfall estimates are available at three levels, known as near-real-time, real-time, and standard products. The near-real-time and real-time GSMaP products are available to the public with 0 and 4 hours latency, respectively (Kubota et al. 2020). The GSMaP_MVK and the GSMaP_Gauge is categorized as the standard product with 3 days latency. The GSMaP_Gauge (defined as GSMaP_G in figures) and GSMaP_MVK version 7 rainfall products are used in this study available from JAXA webpage (https://www.gportal.jaxa.jp/gp). In the version 7 algorithm, the orographic rainfall estimation method by Yamamoto et al. (2017) was used for all sensors (Kubota et al. 2020). The GSMaP_Gauge is adjusted by the global rain gauges derived from the NOAA/CPC, while the GSMaP_MVK is without rain gauges adjustments. Both products have the same spatial and temporal resolution, which is 0.1 degree and 1 hour with coverage between 60°N and 60°S. The KSNDMC gauges are not part of NOAA/CPC gauges.

2.3 IMERG Rainfall

The IMERG rainfall product has been developed as the United States GPM standard product (Huffman et al. 2020), and the IMERG has several advantages over other satellite rainfall products, such as wide spatial representation (60°N – 60°S) of precipitation, fine spatio-temporal resolutions and additional snowfall observations

(Anjum et al. 2018). The IMERG rainfall is the combination of features of three multi-satellite precipitation products including (1) TMPA, (2) CMORPH, and (3) PERSIANN (Precipitation Estimation from Remotely Sensed Information using Artificial Neural Networks; Sorooshian et al. 2000). IMERG product used all constellations of microwave sensors, IR-based observations from geosynchronous satellites and monthly gauge precipitation data from GPCC rain-gauges (Schneider et al. 2014) to correct the bias of satellite retrievals over the land (Huffman et al. 2015, 2020; Sharifi et al. 2018). IMERG rainfall estimates are available at three levels, known as early, late and final stage IMERG products. Early and Late IMERG products provide near real-time rainfall estimates, and are available to the public with 6 and 18 hours latency, respectively (Tan and Duan 2017). The final product is calibrated with the GPCC monthly data, and provides post real-time rainfall estimates after around 4 months of data retrieval. All IMERG products are available at same spatial (0.1°) and temporal (half-hourly, daily and monthly temporal scales) resolutions. The IMERG final products with 30 minutes frequency are used in this study.

3. Methodology

The data assimilation for most weather applications is usually an under-sampling problem in which numbers of grid points are higher on the analysis grid (e.g. satellite retrievals) than observations (here rain gauges) (Daley, 1997). In the direct assimilation systems, like Cressman analysis (Cressman, 1959) or successive correction methods (Bratseth, 1986) in objective analysis, observation information is simply spread to the analysis grid point through interpolation of observation within a radius of influence (ROI) without considering inconsistencies (both observation and background errors) in input parameters. Whereas, the objective of the optimal interpolation and variational method are to minimize the cost function that measures the distance between background (here satellites derived rainfall) and observation (here rain gauge) (Daley, 1997). The variational method spreads observation information to analyze grid points using iterative minimization of the cost function and based upon the background and observation error. The background and observation errors are uncertainties in the satellite and rain gauge data, respectively. An optimal analysis can be prepared using 2D-Var assimilation method by an accurate specification of covariance matrices, due to strong dependence upon these error covariances (Xie et al. 2002; Tyndall 2008, 2010).

The variational technique minimizes a cost function iteratively to compute analysis (x_a). In 2D-Var methodology, the cost (penalty) function $J(x_a)$ is made up of two components:

$$J(x_a) = J_b + J_o \tag{1}$$

where, the term J_b penalizes the analysis for differences between the analysis (x_a) and the GSMaP rainfall considered here as a background field, and the term J_o penalizes the analysis for the difference between the analysis (x_a) and the rain gauge observations defined as:

$$2\,J(x_a) = (x_a - x_b)^T P_b^{-1}(x_a - x_b) \quad + (H(x_a) - y_o)^T P_o^{-1}(H(x_a) - y_o) \tag{2}$$

where, x_a is the analysis variable, x_b is the background field taken from GSMaP_Gauge or GSMaP_MVK rainfall product, P_b and P_o are the background and observation error covariances respectively, y_o is the observation vector taken from rain gauge observations, and H is the forward transform interpolation operator which interpolates analysis grid points to the observation values. Initially, background and observation error covariance are considered as diagonal matrices with values of fixed diagonal elements as 4 mm day^{-1} and 1 mm day^{-1}, respectively. The computational expense of the analysis can be reduced by reformulating the variational equation (2) in observation space using Shermon-Morrision-Woodbury Inversion formula (Lorenc 1986). Equation (2) should be minimized with respect to analysis (x_a) to find the minimum penalty between the GSMaP rainfall and gauge observations:

$$\frac{\partial}{\partial x_a} J(x_a) = 0 \tag{3}$$

The analysis solution is given as

$$x_a = x_b + P_b\ H^T \mu \quad \text{and} \quad y_o - H(x_b) = \left(HP_b\ H^T + P_o\ \right)\mu \tag{4}$$

or equivalently, $x_a = x_b + K_t\left(y_o - H(x_b)\right)$ and $K_t = P_b\ H^T\left(HP_b\ H^T + P_o\ \right)^{-1}$ (5)

Here, K_t is known as Kalman gain at *t* time step.

Further, in place of using fixed diagonal background error covariance, Kalman filter method is implemented to update background error at *t* time step.

$$P_a^t = (I - K_t H_t) P_b^t \tag{6}$$

Here, P_a^t and P_b^t are analysis and background error at *t* time step, H_t is forward transform operator at time *t.* Initially at first time-step, P_b^t is considered as a fixed diagonal matrix. The estimated analysis error (P_a^t) obtained from equation (6) is used to compute background error for *t*+1 time-step using

$$\widehat{P_b^{t+1}} = M P_a^t M^T + Q \tag{7}$$

In this study, *M* is considered as an identity matrix and *Q* is considered as zero matrix for simplicity and complex behavior of rainfall prediction, and may be a scope for future research.

Further, a hybrid background error is used for 2D-Var assimilation in which updated background error is computed using

$$P_b^{t+1} = w_1 \times P_b^{t=0} + w_2 \times \widehat{P_b^{t+1}} \quad , where \;\; w_1 = 0.3\, , and \;\; w_2 = 0.7 \tag{8}$$

Finally, the hybrid assimilation method is performed here to generate merge rainfall product using 2D-Var method with the flow dependent background error matrix using Kalman filter.

3. Results and Discussions

3.1. Comparison of GSMaP_MVK and GSMaP_Gauge rainfall against KSNDMC gauges

The spatial distribution of mean rainfall (in mm day^{-1}) during JJAS from KSNDMC gauges, GSMaP_Gauge V7, and GSMaP_MVK V7 rainfall product for the year 2016—2018 is shown in Fig. 2. The all India (southern peninsula) rainfall in 2016, 2017 and 2018 was 97 (92), 95 (100) and 91 (98) percent of the long period average (LPA; the average rainfall recorded during the months from June to September in the past 50-year period) rainfall from IMD gauges, respectively (IMD Annual Report; www.imd.gov.in). The years of 2016-2018 represent varying rainfall distribution over the Western Ghats from deficit, normal and above normal in years 2016, 2017 and 2018, respectively (Figs. 2a-2c). Large differences are observed in spatial rainfall distribution during years 2017 and 2018 over the Western Ghats and NIK regions, whereas both years are normal rainfall years according to IMD LPA rainfall. Figures 2a-2c show that in general high rainfall observed in the Coastal and Malnad regions during JJAS. However, the mean rainfall is less over NIK and SIK regions due to their occurrence in rain shadow regions of the Western Ghats. The spatial distribution of the GSMaP_Gauge rainfall for the same JJAS period for 2016

(Fig. 2d), 2017 (Fig. 2e) and 2018 (Fig. 2f) suggest that GSMaP_Gauge rainfall products have less error as compared to gauge observations. However, the large magnitudes of rainfall over the Western Ghats regions are underestimated in the GSMaP_Gauge rainfall product. It suggests a need of correction in GSMaP rainfall product over mountainous regions. Takido et al. (2016) also detected that GSMaP_Gauge still underestimated the precipitation intensity in high-elevation regions over Japan. Authors suggested improvements with higher resolution gauge-based network data than the NOAA/CPC gauge data. Similarly, inadequate distributions of the NOAA/CPC gauge data can lead to the underestimation of the rainfall over the Western Ghats regions (Fig. 1a). The spatial distribution of GSMaP_MVK rainfall (Figs. 2g-2i) suggests that this rainfall product has less skill over the orographic heavy rainfall regions. In comparison to GSMaP_Gauge rainfall product (Figs. 2d-2f) which has less error against KSNDMC gauges, GSMaP_MVK rainfall product has slightly higher error against KSNDMC gauges over the Malnad and coastal regions. Both GSMaP_Gauge and GSMaP_MVK rainfall products are able to capture low rainfall over the NIK and SIK regions. These analyses suggest that both rainfall products need further improvement in general and over the mountainous regions, in particular. As noted in Section 2.2, the rainfall estimates over the orographic heavy rainfall regions are inherently problematic and the orographic rainfall estimation methods have been developed and installed in the GSMaP PMW algorithm. Hirose et al. (2019) showed that the GSMaP PMW algorithm with the orographic rainfall estimation method were able to estimate the heavy rainfall band well, but the issue persists in the GSMaP due to unavailability of microwave satellite measurements. Nevertheless, the current results suggest the methods need to be improved further through some more suitable data driven analysis such as hybrid assimilation method.

Further, the BIAS (mean difference), NBIAS (BIAS normalized by total rainfall) and RMSD (root-mean-square difference) statistics used for error estimations are defined as

$$BIAS = \frac{1}{N}\sum_{i=1}^{N}\left(rain_i^{sat} - rain_i^{gauge}\right) \quad (9)$$

$$NBIAS = \frac{1}{N}\sum_{i=1}^{N}\left(\frac{rain_i^{sat} - rain_i^{gauge}}{rain_i^{sat} + rain_i^{gauge}}\right) \quad (10)$$

$$RMSD = \sqrt{\frac{1}{N}\sum_{i=1}^{N}\left(rain_i^{sat} - rain_i^{gauge}\right)^2} \quad (11)$$

where, $rain_i^{sat}$ and $rain_i^{gauge}$ represent rainfall from GSMaP rainfall product and KSNDMC gauge observations, respectively. The total number of data points represented by *N*. Figure 3 shows the scatter plot of GSMaP_Gauge (upper panel) and GSMaP_MVK (lower panel) rainfall product against KSNDMC rain gauges for JJAS 2016—2018. The blue and red lines represent the 45° reference line and best fit line using least square method, respectively. The value of RMSD is 9.5, 10.4 and 12.2 mm day^{-1} for 2016, 2017 and 2018, respectively, when GSMaP_Gauge rainfall product is compared with KSNDMC gauge observations (Figs. 3a-3c). The value of BIAS is 0.5, -0.1, and -1.3 mm day^{-1} for these years, respectively, with correlation of around 0.7. The numbers of collocations are around 0.7 to 0.8 million for the years of 2016-2018. The value of RMSD (BIAS) is 12.1 (-1.7), 12.8 (-1.6), and 16.2 (-1.9) mm day^{-1} for JJAS 2016, 2017, and 2018, respectively in GSMaP_MVK rainfall product (Figs. 3d-3f). Slightly less correlation (~ 0.51) is found in GSMaP_MVK rainfall product as compared to GSMaP_Gauge rainfall product that suggest the importance of gauge calibration in the GSMaP_Gauge rainfall product. Moreover, these statistics are almost similar for different monsoon years (varies from deficit to above normal years) that suggest some inherent limitations of the both selected GSMaP rainfall product over the Karnataka region. The daily area average rainfall variation from KSNDMC rain gauges, and corresponding GSMaP_Gauge and GSMaP_MVK rainfall product for JJAS 2016—2018 suggests that slightly larger errors are found in the GSMaP_MVK rainfall product as compared to GSMaP_Gauge rainfall product. It is important to mention here that both operational GSMaP rainfall products are able to capture the active and break phase of diverse monsoon years (Figure not shown).

To evaluate errors in both operational GSMaP rainfall products, comparison of GSMaP rainfall is extended for different IMD rainfall classification. These IMD rainfall classifications are majorly based on intensity of daily rainfall and it divides daily rainfall into eight different categories varying from *no rain* to *extremely heavy rain* (Table 1; IMD Glossary). Figure 4 shows RMSD and NBIAS in both operational GSMaP rainfall products during JJAS 2016—2018. Results suggest that RMSD varies from 2-13 mm day^{-1} for no rain, very light rain, light rain, and moderate rain classifications (Fig. 4a). A negative NBIAS is found for different rainfall classifications except no rain and very light rain classifications (Fig. 4b). The negative values of NBIAS suggests underestimation of rainfall in both operational GSMaP rainfall products as compared to KSNDMC gauge observations. For light, moderate, rather heavy and heavy rain classifications, GSMaP_Gauge product have less NBIAS as compared to GSMaP_MVK rainfall for all years of 2016-2018. It is important to mention that for few pixels, GSMaP rainfall products also incorrectly classify *no rain* regions as rainy pixels. The RMSD values are very high for rather heavy, heavy rain, very heavy rain, and extremely heavy rain classifications, and ranges from 50-250 mm day^{-1} with negative values of NBIAS (-0.4 to -0.7 for

GSMaP_MVK rainfall). It also suggests that both operational GSMaP rainfall products are erroneous mainly over orographic heavy rainfall regions, which are prone to heavy rainfall over Karnataka. Moreover, the GSMaP_Gauge rainfall product has less RMSD and NBIAS as compared to GSMaP_MVK rainfall product for different rainfall classifications, except very heavy and *extremely heavy rainfall* classifications. The density plot of both operational GSMaP rainfall product against KSNDMC gauges also suggest that GSMaP_Gauge rainfall is closer to observations for low rainfall threshold (< 20 mm day^{-1}), whereas both operational GSMaP rainfall products have almost same distribution for high rainfall thresholds, far from gauges (Figure not shown). It suggests that sparse network of rain gauges over mountainous regions, reduces accuracy of GSMaP_Gauge over Western Ghats region.

The error statistics of both operational GSMaP rainfall products for different regions are presented in Table 2. Results suggest that GSMaP_MVK rainfall has large negative BIAS (13 to 25 mm day^{-1}) over the coastal region with the value of RMSD varying from 25 to 38 mm day^{-1}. The correlation coefficient is around 0.58, 0.37, and 0.58 for years 2016, 2017, and 2018, respectively. The values of NBIAS are high for coastal regions in year 2018 as compared to year 2016. The large BIAS is corrected in GSMaP_Gauge rainfall product over the coastal region to some extent, and values of BIAS (1 to 8 mm day^{-1}) and RMSD (18 to 25 mm day^{-1}) are improved significantly for the years of 2016-2018. Similar to the coastal region, Malnad region (Fig. 1a) also shows large errors in both operational GSMaP rainfall products. The values of BIAS, NBIAS and RMSD are slightly less in Malnad region as compared to coastal region, but correlation coefficient is less for different years. Both NIK and SIK regions show less error in GSMaP rainfall products. The value of RMSD (BIAS) is less than 10 (1) mm day^{-1} for different years and correlation coefficient is around 0.6. For the years of 2016-2018, GSMaP_Gauge data have better skill as compared to GSMaP_MVK rainfall in NIK and SIK regions, which confirms its superiority for all regions due to calibration of GSMaP_Gauge rainfall with the NOAA gauge analysis (Fig. 1a).

These preliminary verification results suggest the need for further rain gauge adjustment of GSMaP rainfall over Malnad and coastal regions. The hybrid assimilation method is implemented here to generate new GSMaP rainfall product over Karnataka, southwestern India. The verification of new GSMaP rainfall products is presented in the next sub-section.

3.2. Evaluation of GSMaP_MVK_NEW and GSMaP_Gauge_NEW rainfall

The randomly selected 50% rain gauges (defined as training gauges) from the average network of around 6100 rain gauges over Karnataka are used to prepare new merge GSMaP rainfall product (defined as GSMaP_Gauge_NEW and GSMaP_MVK_NEW) using hybrid assimilation method. In this hybrid method, a variational method is used to prepare gauge-adjusted GSMaP rainfall and Kalman filter is used to estimate flow of background error in satellite rainfall (discussed in Section 3). The remaining 50% rain gauges (defined as verification gauges) are used for independent verification of different rainfall products. Figure 5 shows the scatter plot of GSMaP_Gauge, GSMaP_Gauge_NEW, GSMaP_MVK, GSMaP_MVK_NEW against training gauges, which are used to prepare GSMaP_Gauge_NEW (Figs. 5b,f,j) and GSMaP_MVK_NEW (Figs. 5d,h,l) rainfall product. The error statistics provide the sanity check to recognize that after merging training gauges in both operational GSMaP rainfall products, the new rainfall products are closer to observations and demonstrate successful assimilation of the training gauges. Results suggest that GSMaP_Gauge rainfall has RMSD (BIAS) of 9.6 (0.4), 10.5 (-0.2), and 12.5 (-1.4) mm day^{-1} for JJAS 2016 (Fig. 5a), 2017 (Fig. 5e), and 2018 (Fig. 5i), respectively. These error statistics are reduced to 3.9 (0.1), 4.2 (-0.0), and 4.7 (-0.2) mm day^{-1}, respectively for JJAS 2016 (Fig. 5b), 2017 (Fig. 5f), and 2018 (Fig. 5j). The values of BIAS are close to zero after hybrid assimilation due to the bias correction step implemented in the variational assimilation method. The value of correlation coefficient has increased from around 0.7 in GSMaP_Gauge to 0.96 in GSMaP_Gauge_NEW rainfall. The number of training gauges observations are almost 0.35 million for different years. These statistics suggest that after merging of training gauges in GSMaP rainfall product by hybrid assimilation method, new rainfall products are closer to training gauges and supports successful ingestion of ground observations. Similar to GSMaP_Gauge rainfall product, error statistics for GSMaP_MVK rainfall product is also improved from 12.3 (-1.8), 13.0 (-1.6), and 16.5 (-2.1) mm day^{-1} for JJAS 2016 (Fig. 5c), 2017 (Fig. 5g), and 2018 (Fig. 5k), respectively to 4.1 (-0.2), 4.4 (-0.2), and 4.9 (-0.3) mm day^{-1} in GSMaP_MVK_NEW (Figs. 5d,h,l) rainfall product. The value of correlation coefficient is also improved from around 0.52 in GSMaP_MVK rainfall product to 0.96 in GSMaP_MVK_NEW rainfall product. These statistics suggest that after merging of training gauges with GSMaP_MVK rainfall product, the new rainfall products are closer to assimilated observations (training gauges) and support successful assimilation of the ground observations.

After initial verification of operational and new GSMaP rainfall products, these rainfall products are also compared with verification gauges that can be considered as independent verification. Results suggest that GSMaP_Gauge rainfall has RMSD (BIAS) of 9.4 (0.5), 10.3 (-0.1), and 11.9 (-1.2) mm day^{-1} for JJAS 2016 (Fig. 6a), 2017 (Fig. 6e), and 2018 (Fig. 6i), respectively. These error statistics are changed to 6.8 (0.1), 7.4 (-0.1), and 8.1 (-0.4) mm day^{-1}, respectively in GSMaP_Gauge_NEW rainfall product for JJAS 2016 (Fig. 6b), 2017 (Fig. 6f), and 2018 (Fig. 6j). The value of correlation coefficient has increased from around 0.7 in GSMaP_Gauge to 0.86 in GSMaP_Gauge_NEW rainfall. The numbers of verification gauges are almost similar to the number of training gauges for different years. These results suggest that new rainfall products have less error as compared to operational GSMaP rainfall products when compared with verification gauges. Similar to GSMaP_Gauge rainfall product, error statistics for GSMaP_MVK rainfall product is also improved from 11.9 (-1.6), 12.7 (-1.5), and 15.6 (-1.8) mm day^{-1} for JJAS 2016 (Fig. 6c), 2017 (Fig. 6g), and 2018 (Fig. 6k), respectively to 7.4 (-0.4), 8.2 (-0.5), and 8.9 (-0.5) mm day^{-1} in GSMaP_MVK_NEW (Figs. 6d,h,l) rainfall product. The values of correlation coefficient are also improved from around 0.53 in GSMaP_MVK rainfall product to around 0.82 in GSMaP_MVK_NEW rainfall product. These statistics suggest that new rainfall products have better statistics with verification gauges as compared to GSMaP_MVK operational rainfall product. It is also important to discuss here that the larger improvements are found in GSMaP_MVK rainfall product as compared to GSMaP_Gauge rainfall product that may be due to calibration of GSMaP_Gauge rainfall with the NOAA/CPC gauges in operational production.

Figure 7 shows the spatial distribution of the improvement parameter (*IP*) for GSMaP_Gauge_NEW and GSMaP_MVK_NEW rainfall product compared to operational GSMaP_Gauge and GSMaP_MVK rainfall product when compared with verification gauges. The *IP* is defined as

$$IP = \left|\frac{1}{N}\sum_{i=1}^{N} \left(GSMaP_{GaugeorMVK} - KSNDMC_{ver}\right)\right| - \left|\frac{1}{N}\sum_{i=1}^{N} \left(GSMaP_{Gauge\_NEWorMVK\_NEW} - KSNDMC_{ver}\right)\right| \quad (12)$$

where, GSMaP_Gauge or GSMaP_MVK rainfall product is defined as $GSMaP_{GaugeorMVK}$, GSMaP_Gauge_NEW or GSMaP_MVK_NEW rainfall product is defined as $GSMaP_{Gauge\_NEWorMVK\_NEW}$, total number of collocations are defined as *N*, verification gauges are defined as $KSNDMC_{ver}$. The positive (negative) value of *IP* corresponds to improvement (degradation) of the GSMaP_Gauge_NEW or GSMaP_MVK_NEW rainfall product as compared to GSMaP_Gauge or GSMaP_MVK rainfall product. Figures 7a-7c show positive value of improvement parameters over Karnataka for the years of 2016-2018. These improvements are more prominent over the Western Ghats region for GSMaP_Gauge rainfall with few pockets of degradation. The domain average value of *IP* is positive that suggests that quality of GSMaP rainfall products are improved with the ingestion of training gauges when compared with verification gauges. These positive improvements are more prominent for GSMaP_MVK rainfall products (Figs. 7d-7f) that may be due to absence of the NOAA gauge calibration in this rainfall product. The spatial distribution of *IP* for different years suggests that the maximum positive impact is observed over the Western Ghats regions. The values of *IP* for GSMaP_Gauge_NEW are largest for JJAS 2018 and smallest for JJAS 2016 over the Western Ghats. However, the values of *IP* are almost similar for GSMaP_MVK_NEW rainfall for different years. Results also suggest that in addition to coastal and Western Ghats regions, NIK and SIK regions show improvement for different years.

In addition to comparison of different rainfall products against verification gauges, these new rainfall products are also compared with IMERG final rainfall product. IMERG final rainfall product uses GPCC gauge analysis to calibrate merge rainfall products. As described in Schneider et al. (2014), the GPCC uses two rain gauge sources in addition to the NOAA CPC (used in the GSMaP). Dinku et al. (2008) found that the GPCC product has better overall statistics as compared to the NOAA CPC over a mountainous region of Africa. Earlier studies suggest that IMERG final products have sufficient skill over tropical regions and this dataset can be considered as an independent source for verification. The JAXA operational and new GSMaP rainfall products are also compared with IMERG final rainfall products for years 2016—2018. Results suggest that GSMaP_Gauge rainfall has RMSD (BIAS) of 9.8 (-0.6), 8.8 (0.0), and 8.8 (-0.5) mm day^{-1} for JJAS 2016 (Fig. 8a), 2017 (Fig. 8e), and 2018 (Fig. 8i), respectively. These error statistics are changed to 9.9 (-0.9), 9.3 (0.0), and 9.9 (0.4) mm day^{-1}, respectively for JJAS 2016 (Fig. 8b), 2017 (Fig. 8f), and 2018 (Fig. 8j). The value of correlation coefficient is slightly more for GSMaP_Gauge_NEW as compared to GSMaP_Gauge rainfall. However, slightly larger values of RMSD and BIAS are found in new rainfall products as compared to operational GSMaP rainfall products. These results suggest that new rainfall products have negligible to very small changes as compared to operational GSMaP rainfall products when compared with IMERG final rainfall. The error statistics for GSMaP_MVK rainfall product is improved from 10.9 (-2.7), 9.7 (-1.4), and 13.2 (-1.1) mm day^{-1} for JJAS 2016 (Fig. 8c), 2017 (Fig. 8g), and 2018 (Fig. 8k), respectively to 9.9 (-1.5), 9.2 (-0.4), and 10.3 (0.3) mm day^{-1} in GSMaP_MVK_NEW (Figs. 8d,h,l) rainfall product. The values of correlation coefficient are also improved from around 0.64 in GSMaP_MVK rainfall product to around 0.71 in GSMaP_MVK_NEW rainfall product for JJAS 2016 and 2017, with larger improvements in JJAS 2018. These statistics suggest that new rainfall products have less error with IMERG final data as compared to GSMaP_MVK operational rainfall product. It is also important to discuss here that the large improvements are found in GSMaP_MVK rainfall when compared with IMERG final data, whereas, negligible to little changes are found for GSMaP_Gauge rainfall. It is important to mention here that the new GSMaP rainfall products have higher correlation with verification gauges as well as IMERG final data that supports the improved skill of rainfall product after hybrid assimilation of training gauges.

To evaluate the skill of operational and new GSMaP rainfall products, these data are also compared with verification gauges for different IMD classifications. In addition to *IP* defined in equation (12), absolute NBIAS are also used to understand the quality of new rainfall products as compared to operational GSMaP rainfall products. The absolute NBIAS parameter is defined as

$$Absolute\ NBIAS = \left| \frac{1}{N} \sum_{i=1}^{N} \left(\frac{GSMaP_{GaugeorMVK} - KSNDMC_{ver}}{GSMaP_{GaugeorMVK} + KSNDMC_{ver}} \right) \right| - \left| \frac{1}{N} \sum_{i=1}^{N} \left(\frac{GSMaP_{Gauge_{NEW} or MVK_{NEW}} - KSNDMC_{ver}}{GSMaP_{Gauge_{NEW} or MVK_{NEW}} + KSNDMC_{ver}} \right) \right| \quad (13)$$

Positive (negative) values of absolute NBIAS show improvement (degradation) of new rainfall data against operational GSMaP rainfall. Figure 9 shows improvement parameter and absolute NBIAS in both GSMaP_Gauge_NEW and GSMaP_MVK_NEW rainfall products during JJAS 2016—2018. Results suggest that the value of improvement varies from 2-60 mm day^{-1} for different rain classifications (Fig. 9a). Generally, GSMaP_Gauge rainfall has less improvement as compared to GSMaP_MVK rainfall product. It suggests that due to operational gauge calibration, GSMaP_Gauge rainfall product is closer to ground observations. It is also important to note that for all heavy rainfall classifications, both operational GSMaP rainfall products show large improvement (Fig. 9a). These large improvements are mainly over the Western Ghats regions, and more noteworthy for years 2017 and 2018. The value of absolute NBIAS in GSMaP_Gauge is less as compared to GSMaP_MVK for different rainfall classifications except very heavy and extremely heavy rainfall classifications (Fig. 9b). These results suggest substantial improvement in operational GSMaP rainfall product after implementing hybrid assimilation. It is also important to note that the areas with higher precipitation show larger improvement.

The density plot of rainfall deviation (defined as GSMaP minus rain gauge) for GSMaP_Gauge, GSMaP_Gauge_NEW, GSMaP_MVK, and GSMaP_MVK_NEW for years 2016—2018 are shown in Fig. 10. This figure suggests that for different rainfall thresholds GSMaP_Gauge_NEW and GSMaP_MVK_NEW rainfall have less error. The new product is closer to observations for all years as compared to operational GSMaP rainfall products. The density plot of deviation is shifted towards low rainfall values that suggest that more numbers of points are closer to observations after assimilation. However, for high rainfall thresholds both operational GSMaP rainfall products have large deviations. It suggests that a dense network of rain gauges over orographic heavy rainfall regions improves the quality of both operational GSMaP rainfall products. Results also present better performance of GSMaP_Gauge as compared to GSMaP_MVK rainfall product for selected study period. Moreover, new rainfall products have better skill for high rainfall thresholds over Karnataka, India. The hybrid assimilation of additional gauge observations mainly over the Western Ghats regions are able to capture magnitude of the complete dynamical range of rainfall (mainly higher rainfall) accurately as compared to operational GSMaP rainfall products.

3.3. Evaluation of different assimilation method for variable density of rain gauges

The Cressman (Cressman, 1959) and optimal interpolation (Daley, 1997) methods are also used in this study in addition to hybrid assimilation method to understand the importance of the hybrid assimilation method. To recognize the need of dense rain gauge network, total rain gauge stations in the year 2018 are randomly divided as training and validation gauge stations. Further, the training gauge stations used for data assimilation are divided in three cases viz. RG1 (all training rain gauge stations), RG2 (50% of training rain gauge stations), and RG3 (25% of training rain gauge stations). Merge rainfall product prepared from different assimilation methods (viz. Cressman, Optimal interpolation and hybrid method) and variable numbers of rain gauge stations (viz. RG1, RG2, and RG3) in addition to both operational GSMaP rainfall products are compared with independent validation rain gauge stations for ISM 2018. The radius of influence (ROI) is considered as 5 km for Cressman method. The fix observation and background error for optimal interpolation method is same as used for variational assimilation discussed in section 3. The RMSD values for RG1, RG2, and RG3 with different assimilation methods are shown in Table 3.

Results show that in general merge rainfall products have less error as compared to both operational GSMaP products. Less RMSD values are noticed in optimal interpolation method as compared to Cressman method. The reduction of RMSD is more in hybrid assimilation method as compared to other selected assimilation methods. It clearly shows the importance of considering flow of background error covariance in hybrid assimilation method that considered as fix in optimal interpolation method (i.e. B is considered as diagonal matrices with diagonal elements as 4 mm day^{-1} in optimal interpolation method). Additionally, high-density rain gauge network has large impact on merge rainfall product. The RMSD values of 11.8 (15.3), 11.4 (14.6), and 10.7 (12.8) mm day^{-1} are noticed in the Cressman method generated merge GSMaP_Gauge (GSMaP_MVK) product for RG3, RG2, and RG1 gauges, respectively. It is also important to mention here that both rain gauge density and assimilation methodology are important for preparing merge rainfall products. Cressman and optimal interpolation methods show more effect of dense gauge network for GSMaP_MVK rainfall products. The values of RMSD are reduced from 15.3 (13.1) to 12.8 (9.4) mm day^{-1} for Cressman (optimal interpolation) method in GSMaP_MVK rainfall for RG3 to RG1 gauges, respectively. However, the impact of the utilized rain gauge numbers is relatively less in hybrid assimilation method. The values of RMSD is changed from 10.6 to 8.3 mm day^{-1} for RG3 to RG1 gauges in GSMaP_MVK merge rainfall for hybrid assimilation method. In general, the RMSD values are less in GSMaP_Gauge product, that signify the importance of operational gauge calibration used in this product.

4. Conclusions

A hybrid assimilation method for merging various rainfall products over a unique-site with dense gauge observations network over Karnataka region of southwestern India has been developed and demonstrated. The verification results for four topographically different regions within study area suggest a large error in GSMaP rainfall over coastal and Malnad Western-Ghat area, a windward side of the mountainous regions, whereas GSMaP rainfall is able to capture rainfall patterns over NIK and SIK regions. The GSMaP_Gauge rainfall product has more skill as compared to GSMaP_MVK rainfall over orographic heavy rainfall regions, and the former has less RMSD and higher correlation. Present results reconfirm large errors for high rainfall threshold for different IMD rainfall classifications. These preliminary verifications at daily scale with an independent dense gauge network suggest that further plausible modifications are possible in operational GSMaP rainfall products using ground observations mainly over orographic heavy rainfall regions, the areas well known for their land inhomogeneity. A hybrid assimilation method is implemented as a combination of variational method and Kalman filter method, in which rain gauge observations are used to prepare analysis that is an optimal combination of ground observations and GSMaP rainfall product, and evolution of background error is simulated using Kalman filter. Results suggest that new GSMaP rainfall analyses are closer to gauge observations, which are used for optimally combining and show successful assimilation of gauge observations. Further, these new daily rainfall products are compared with independent gauge observations and IMERG final rainfall products calibrated by the GPCC. Results suggest that the new analyses are in better agreement with the independent observations. Moreover, the distributions of new rainfall products match well with gauge observations. Results are also extended to understand the importance of dense rain gauge network and different data assimilation methods like Cressman method, optimal interpolation method in addition to hybrid assimilation method. These results suggest that both dense rain gauge network and assimilation methods are important for preparing merge rainfall products. The hybrid assimilation method shows less error as compared to Cressman and optimal interpolation methods for the impacts of the utilized rain gauge numbers. In all cases, GSMaP_Gauge has less error as compared to GSMaP_MVK rainfall product. These analyses suggest that an optimal number of ground-based observations with hybrid assimilation methods have greater potential to improve satellite-based rainfall estimates. Development of this new daily gridded rainfall product can be used for various agricultural, hydrological, and meteorological applications. Moreover, such a merged product is also useful for data assimilation in the weather models (Kumar 2020), verification of model skills, monitoring of the monsoon progress and its assessment (in terms of its active and break phases), calculation of fresh water fluxes over the oceans, etc. In the present hybrid assimilation method, variation of background error with model error is not considered that may be a scope for future research. Moreover, precise estimation of observation error is also a challenging issue that is considered here as a fixed diagonal matrix. The scope of this study can be further extended with the augmentation in terms of the finer temporal resolution from daily scale to hourly scale for various hydro-meteorological applications.

Acknowledgments

The authors are thankful to the Director, Space Applications Centre, ISRO, India. The authors are also thankful to the Deputy Director, EPSA, Space Applications Centre, ISRO, India. Thanks are also due to the KSNDMC team for providing the rain gauge observations used in this study. The research described in this paper was carried out under the Implementation Arrangement between the ISRO and the JAXA concerning collaborative activities on improved rainfall products. Authors are also thankful to two anonymous reviewers for their valuable suggestions.

References

Adler, R. F., G. J.Huffman, A. Chang, R. Ferraro, P. P. Xie, J.Janowiak, B. Rudolf, U. Schneider, S. Curtis, D. B. A. Gruber, J. Susskind, P. Arkin, and E.Nelkin, 2003: The version-2 global precipitation climatology project (GPCP) monthly precipitation analysis (1979–present). *J. Hydrometeor.,***4**, 1147-1167.

Anjum, M. N., Y. Ding, D. Shangguan, I. Ahmad, M. W. Ijaz, H. U. Farid, Y. E. Yagoub, M. Zaman, and M. Adnan, 2018: Performance evaluation of latest integrated multi-satellite retrievals for Global Precipitation Measurement (IMERG) over the northern highlands of Pakistan. *Atmospheric research*, **205**, 134-146.

Aonashi, K., J. Awaka, M. Hirose, T. Kozu, T. Kubota, G. Liu, S. Shige, S. Kida, S. Seto, N. Takahashi, and Y. N. Takayabu, 2009: GSMaP passive microwave precipitation retrieval algorithm: Algorithm description and validation. *Journal of the Meteorological Society of Japan. Ser. II*, **87**, 119-136.

Attada, R., P. Kumar, and H. P. Dasari, 2018: Assessment of land surface models in a high-resolution atmospheric model during Indian summer monsoon. *Pure Appl. Geophys.,* **175**, 3671-3696.

Bianchi, B., P. J.V. Leeuwen, R. J. Hogan, and A. Berne, 2013: A variational approach to retrieve rain rate by combining information from rain gauges, radars, and microwave links. *J. Hydrometeor.,* **14**, 1897-1909.

Bratseth, A. M., 1986: Statistical interpolation by means of successive corrections. *Tellus A*, **38**, 439-447.

Brocca, L., L. Ciabatta, C. Massari, T. Moramarco, S. Hahn, S. Hasenauer, R. Kidd, W. Dorigo, W. Wagner, and V. Levizzani, 2014: Soil as a natural rain gauge: Estimating global rainfall from satellite soil moisture data. *Journal of Geophysical Research: Atmospheres*, **119**, 5128-5141.

Chen, M., W. Shi, P. Xie, V. B. S. Silva, V. E. Kousky, R. Wayne Higgins, and J. E. Janowiak, 2008: Assessing objective techniques for gauge-based analyses of global daily precipitation. *J. Geophys. Res.*, **113**, D04110.

Chen, S., J. Hu, Z. Zhang, A. Behrangi, Y. Hong, A. S.Gebregiorgis, J. Cao, B. Hu, X. Xue, and X. Zhang, 2015: Hydrologic evaluation of the TRMM multisatellite precipitation analysis over Ganjiang Basin in humid southeastern China. *IEEE Journal of Selected Topics in Applied Earth Observations and Remote Sensing*, **8**, 4568-4580.

Cheng, H., M. Jardak, M. Alexe, and A. Sandu, 2010: A hybrid approach to estimating error covariances in variational data assimilation. *Tellus A: Dynamic Meteorology and Oceanography*, **62**, 288-297.

Chiaravalloti, F., L. Brocca, A. Procopio, C. Massari, and S. Gabriele,2018: Assessment of GPM and SM2RAIN-ASCAT rainfall products over complex terrain in southern Italy. *Atmospheric Research*, **206**, 64-74.

Cressman, G. P., 1959: An operational objective analysis system. *Mon. Wea. Rev*, **87**, 367-374.

Daley, R., 1997: Atmospheric Data Assimilation (Special Issue Data Assimilation in Meteology and Oceanography: Theory and Practice). *Journal of the Meteorological Society of Japan. Ser. II*, **75**, 319-329.

Dinku, T., S. J. Connor, P. Ceccato, and C. F. Ropelewski, 2008: Comparison of global gridded precipitation products over a mountainous region of Africa. *International Journal of Climatology*, **28**, 1627-1638.

Gairola, R. M., and T. N. Krishnamurti, 1992: Rain rates based on SSM/I, OLR and raingauge data sets. *Meteorology and Atmospheric Physics*, **50**, 165-174.

Gairola, R. M., S. Prakash, and P. K. Pal, 2015: Improved rainfall estimation over the Indian monsoon region by synergistic use of Kalpana-1 and rain gauge data. *Atmósfera*, **28**, 51-61.

Gairola, R. M., S. Prakash, and C. Mahesh, 2012: Synergistic use of Kalpana-1 and rain gauge data for rainfall estimation: A case study over Gujarat. *Workshop on Meteorological Satellite Kalpana: A decade of Service to the Nation. Ahmedabad,India, October*.

Hirose, H., S. Shige, M. K. Yamamoto, and A. Higuchi, 2019: High temporal rainfall estimations from Himawari-8 multiband observations using the random-forest machine-learning method. *J. Meteor. Soc. Japan*, **97**, 689-710.

Hirose, M., R. Oki, D. A. Short, and K. Nakamura, 2009: Regional characteristics of scale-based precipitation systems from ten years of TRMM PR data. J. Meteor. Soc. Japan, 87A, 353–368, doi:10.2151/jmsj.87A.353.

Hirose, M., Y. N. Takayabu, A. Hamada, S. Shige, M. K. Yamamoto, 2017a: Spatial contrast of geographically induced rainfall observed by TRMM PR. *J. Climate*, **30**, 4165-4184.

Hirose, M., Y. N. Takayabu, A. Hamada, S. Shige, and M. K. Yamamoto, 2017b: Impact of long-term observation on the sampling characteristics of TRMM PR precipitation. *J. Appl. Meteor. Climatol.*,**56**, 713-723.

Hirose, M., and K. Okada, 2018: A 0.01° Resolving TRMM PR Precipitation Climatology. *J. Appl. Meteor. Climatol.*,**57**, 1645-1661.

Hou, A. Y., R. K. Kakar, S.Neeck, A. A.Azarbarzin, C. D. Kummerow, M. Kojima, R. Oki, K. Nakamura, and T. Iguchi, 2014: The global precipitation measurement mission. *Bulletin of the American Meteorological Society*, **95**, 701-722.

Hu, Z., Q. Hu, C. Zhang, X. Chen, and Q. Li, 2016: Evaluation of reanalysis, Spatially-interpolated and satellite remotely-sensed precipitation datasets in central Asia. *Journal of Geophysical Research: Atmospheres*, **121**, 5648–5663.

Huffman, G. J., D. T.Bolvin, E. J. Nelkin, D. B. Wolff, R. F. Adler, G. Gu, Y. Hong, K. P. Bowman, and E. F. Stocker, 2007: The TRMM multisatellite precipitation analysis (TMPA): Quasi-global, multiyear, combined-sensor precipitation estimates at fine scales. *Journal of hydrometeorology*, **8**, 38-55.

Huffman, G. J., D. T. Bolvin, D. Braithwaite, K. Hsu, R. Joyce, P. Xie, and S. H. Yoo, 2015: NASA global precipitation measurement (GPM) integrated multi-satellite retrievals for GPM (IMERG). *Algorithm theoretical basis document,* **4**, 30.

Huffman, G. J., D. T. Bolvin, D. Braithwaite, K.-L. Hsu, R. J. Joyce, C. Kidd, E. J. Nelkin, S. Sorooshian, E. F. Stocker, J. Tan, D. B. Wolff, and P. Xie, 2020: Integrated Multi-satellite Retrievals for the Global Precipitation Measurement (GPM) Mission (IMERG). In: Satellite Precipitation Measurement, Eds., Springer Nature, Cham, *Advances in Global Change Research*, **67**, 343-353.

Joyce, R. J., J. E. Janowiak, P. A. Arkin, and P. Xie, 2004: CMORPH: A method that produces global precipitation estimates from passive microwave and infrared data at high spatial and temporal resolution. *Journal of hydrometeorology*, **5**, 487-503.

Krishnamurti, T. N., A. K. Mishra, A. Simon, and A. Yatagai, 2009: Use of a dense rain-gauge network over India for improving blended TRMM products and downscaled weather models. *Journal of the Meteorological Society of Japan. Ser. II*, **87**, 393-412.

Kubota, T., S. Shige, H. Hashizume, K. Aonashi, N. Takahashi, S. Seto, M. Hirose, Y. N. Takayabu, T. Ushio, K. Nakagawa, and K. Iwanami, 2007: Global precipitation map using satellite-borne microwave radiometers by the GSMaP project: Production and validation. *IEEE Transactions on Geoscience and Remote Sensing*, **45**, 2259-2275.

Kubota, T., T. Ushio, S. Shige, S. Kida, M. Kachi, and K. Okamoto, 2009: Verification of high resolution satellite-based rainfall estimates around Japan using gauge-calibrated ground radar dataset. *J. Meteor. Soc. JapanSer. II*, **87**, 203-222.

Kubota, T., K. Aonashi, T. Ushio, S. Shige, Y. N. Takayabu, M. Kachi, Y. Arai, T. Tashima, T. Masaki, N. Kawamoto, T. Mega, M. K. Yamamoto, A. Hamada, M. Yamaji, G. Liu, and R. Oki, 2020: Global Satellite Mapping of Precipitation (GSMaP) products in the GPM era.*Satellite precipitation measurement*, Volume 1, Springer, Cham.https://doi.org/10.1007/978-3-030-24568-9_20

Kumar, P., 2020: Assimilation of the rain-gauges measurements using Particle Filter. *Earth and Space Science*, **7**, in press.

Kumar, P., C. M. Kishtawal, and P. K. Pal, 2014: Impact of satellite rainfall assimilation on Weather Research and Forecasting model predictions over the Indian region. *Journal of Geophysical Research: Atmospheres*, **119**, 2017-2031.

Li, H., Y. Hong, P. Xie, J. Gao, Z. Niu, P. Kirstetter, and B. Yong, 2015: Variational merged of hourly gauge- satellite precipitation in China: Preliminary results. *Journal of Geophysical Research: Atmospheres*, **120**, 9897-9915.

Lorenc, A. C., 1986: Analysis methods for numerical weather prediction. *Quart. J. Roy. Meteor. Soc.*, **112**, 1177-1194.

Maggioni, V., P. C. Meyers, and M. D. Robinson, 2016: A review of merged high-resolution satellite precipitation product accuracy during the Tropical Rainfall Measuring Mission (TRMM) era. *Journal of Hydrometeorology*, **17**, 1101-1117.

Mega, T., T. Ushio, T. Matsuda, T. Kubota, M. Kachi, and R. Oki, 2019: Gauge-Adjusted Global Satellite Mapping of Precipitation.*IEEE Trans. Geosci. Remote Sens*, **57**, 1928-1935.

Mitra, A. K., M. D. Gupta, S. V. Singh, and T. N.Krishnamurti, 2003: Daily rainfall for the Indian monsoon region from merged satellite and rain gauge values: Large-scale analysis from real-time data. *Journal of Hydrometeorology*, **4**, 769-781.

Mitra, A. K., A. K. Bohra, M. N.Rajeevan, and T. N.Krishnamurti, 2009: Daily Indian precipitation analysis formed from a merge of rain-gauge data with the TRMM TMPA satellite-derived rainfall estimates. *Journal of the Meteorological Society of Japan. Ser. II*, **87**, 265-279.

Mohapatra, G. N., V. Rakesh, and K. V. Ramesh, 2017: Urban extreme rainfall events: categorical skill of WRF model simulations for localized and non-localized events. *Quarterly Journal of the Royal Meteorological Society*, **143**, 2340-2351.

Nodzu, M. I., J. Matsumoto, L. Trinh-Tuan, and T. Ngo-Duc, 2019: Precipitation estimation performance by Global Satellite Mapping and its dependence on wind over northern Vietnam. *Progress in Earth and Planetary Science*, **6**, 58.

Palazzi, E., J. von Hardenberg, and A. Provenzale, 2013: Precipitation in the Hindu-Kush Karakoram Himalaya: Observations and future scenarios. *Journal of Geophysical Research: Atmospheres*, **118**, 85–100.

Prakash, S., A. K. Mitra, A. AghaKouchak, Z. Liu, H. Norouzi,and D. S. Pai, 2018: A preliminary assessment of GPM-based multi-satellite precipitation estimates over a monsoon dominated region. *Journal of Hydrology*, **556**, 865-876.

Roy Bhowmik, S., and A. K. Das, 2007: Rainfall analysis for Indian monsoon region using the merged rain gauge observations and satellite estimates: Evaluation of monsoon rainfall features. *Journal of Earth System Science*, **116**, 187-198.

Schneider, U., A. Becker, P. Finger, A. Meyer-Christoffer, M.Ziese, and B. Rudolf, 2014: GPCC's new land surface precipitation climatology based on quality-controlled in situ data and its role in quantifying the global water cycle.*Theor. Appl. Climatol.*, **115**, 15-40.

Shah, H. L., and V. Mishra, 2016: Uncertainty and bias in satellite-based precipitation estimates over Indian subcontinental basins: Implications for real-time streamflow simulation and flood prediction. *Journal of Hydrometeorology*, **17**, 615–636.

Sharifi, E., R. Steinacker, and B. Saghafian, 2018: Multi time-scale evaluation of high-resolution satellite-based precipitation products over northeast of Austria. *Atmospheric Research*, **206**, 46-63.

Shige, S., T. Yamamoto, T. Tsukiyama, S. Kida, H. Ashiwake, T. Kubota, S. Seto, K. Aonashi, and K. Okamoto, 2009: The GSMaP precipitation retrieval algorithm for microwave sounders. Part I: Over-ocean algorithm. *IEEE Trans. Geosci. Remote Sens.*, **47**, 3084-3097.

Shige, S., S. Kida, H. Ashiwake, T. Kubota, and K. Aonashi, 2013: Improvement of TMI rain retrievals in mountainous areas. *J. Appl. Meteor. Climatol.*,**52**, 242-254.

Shige, S., M. K. Yamamoto, and A. Taniguchi, 2014: Improvement of TMI rain retrieval over the Indian subcontinent. *Remote sensing of the terrestrial water cycle*, geophysical monograph 206, Edited by V. Lakshmi, American Geophysical Union, 27-42.

Shige, S., Y. Nakano, and M. K. Yamamoto, 2017: Role of Orography, Diurnal Cycle, and Intraseasonal Oscillation in Summer Monsoon Rainfall over the Western Ghats and Myanmar Coast. *Journal of Climate*, **30,** 9365-9381.

Singh, A. K., J. N. Tripathi, K. K. Singh, V. Singh, and M. Sateesh, 2019: Comparison of different satellite-derived rainfall products with IMD gridded data over Indian meteorological subdivisions during Indian Summer Monsoon (ISM) 2016 at weekly temporal resolution.*Journal of Hydrology*, **575**, 1371-1379.

Skofronick-Jackson, G., W. A. Petersen, W. Berg, C. Kidd, E. F. Stocker, D. B.Kirschbaum, R. Kakar, S. A. Braun, G. J. Huffman, T. Iguchi, P. E. Kirstetter, C.Kummerow, R. Meneghini, R. Oki, W. S. Olson, Y. Takayabu, K. Furukawa, and T. Wilheit, 2017: The global precipitation measurement (GPM) mission for science and society. *Bull. Amer. Meteor. Soc*., **98**, 1679–1695.

Sorooshian, S., K. L. Hsu, X. Gao, H. V. Gupta, B. Imam, and D. Braithwaite, 2000: Evaluation of PERSIANN system satellite-based estimates of tropical rainfall. *Bulletin of the American Meteorological Society*, **81**, 2035-2046.

Sun, Q., C. Miao, Q. Duan, H. Ashouri, S. Sorooshian, and K. L. Hsu, 2018: A review of global precipitation data sets: Data sources, estimation, and inter-comparisons. *Reviews of Geophysics*, **56**, 79–107.

Takido, K., O. C. Saavedra Valeriano, M. Ryo, K. Tanuma, T. Ushio, and T. Kubota, 2016: Spatiotemporal Evaluation of the Gauge Adjusted Global Satellite Mapping of Precipitation at the Basin Scale.*J. Meteor. Soc. Japan*, **94**, 185-195.

Tan, M., and Z. Duan, 2017: Assessment of GPM and TRMM precipitation products over Singapore. *Remote Sensing*, **9**, 720.

Taniguchi, A., S. Shige, M. K. Yamamoto, T. Mega, S. Kida, T. Kubota, M. Kachi, T. Ushio, and K. Aonashi, 2013: Improvement of high-resolution satellite rainfall product for Typhoon Morakot (2009) over Taiwan. *J. Hydrometeorol.*, **14**, 1859-1871.

Trinh-Tuan, L., J. Matsumoto, T. Ngo-Duc, M. I. Nodzu, and T. Inoue, 2019: Evaluation of satellite precipitation products over Central Vietnam. *Progress in Earth and Planetary Science*, **6**, 54.

Turner, A. G., G. S. Bhat, G. M. Martin, D. J. Parker, C. M. Taylor, A. K. Mitra, S. N. Tripathi, S. Milton, E. N. Rajagopal, J. G. Evans, and R. Morrison, 2019: Interaction of Convective Organisation with Monsoon Precipitation, Atmosphere, Surface and Sea: the 2016 INCOMPASS field campaign in India. *Quarterly Journal of the Royal Meteorological Society*,**146,** 2828– 2852.

Tyndall, D. P., 2008: Sensitivity of surface temperature analyses to specification of background and observation error covariances. Dept. of Meteorology, University of Utah, 98 pp. [http://content.lib.utah.edu/u?/us-etd2,99735.]

Tyndall, D. P., 2010: An investigation of strong and weak constraints to improve variational surface analyses. (Doctoral dissertation, Doctoral dissertation, The University of Utah).

Ushio, T., K. Sasashige, T. Kubota, S. Shige, K. I. Okamoto, K. Aonashi, T. Inoue, N. Takahashi, T. Iguchi, M. Kachi, and R. Oki, 2009: A Kalman filter approach to the Global Satellite Mapping of Precipitation (GSMaP) from combined passive microwave and infrared radiometric data. *Journal of the Meteorological Society of Japan. Ser. II*, **87**, 137-151.

Wang, W., H. Lu, T. Zhao, L. Jiang, and J. Shi, 2017: Evaluation and comparison of daily rainfall from latest GPM and TRMM products over the Mekong River Basin. *IEEE Journal of Selected Topics in Applied Earth Observations and Remote Sensing*, **10**, 2540-2549.

Wang, Z., R. Zhong, C. Lai, and J. Chen, 2017: Evaluation of the GPM IMERG satellite-based precipitation products and the hydrological utility. *Atmospheric Research*, **196**, 151-163.

Xie, Y., C. Lu, and G. L. Browning, 2002: Impact of formulation of cost function and constraints on three-dimensional variational data assimilation. *Mon. Wea. Rev.*, **130**, 2433-2447.

Yamamoto, M. K., and S. Shige, 2015: Implementation of an orographic/nonorographic rainfall classification scheme in the GSMaP algorithm for microwave radiometers. *Atmos. Res.*, **163**, 36-47.

Yamamoto, M. K., S. Shige, C. K. Yu, and L. W. Cheng, 2017: Further improvement of the heavy orographic rainfall retrievals in the GSMaP algorithm for microwave radiometers. *J. Appl. Meteor. Climatol.*,**56**, 2607-2619.

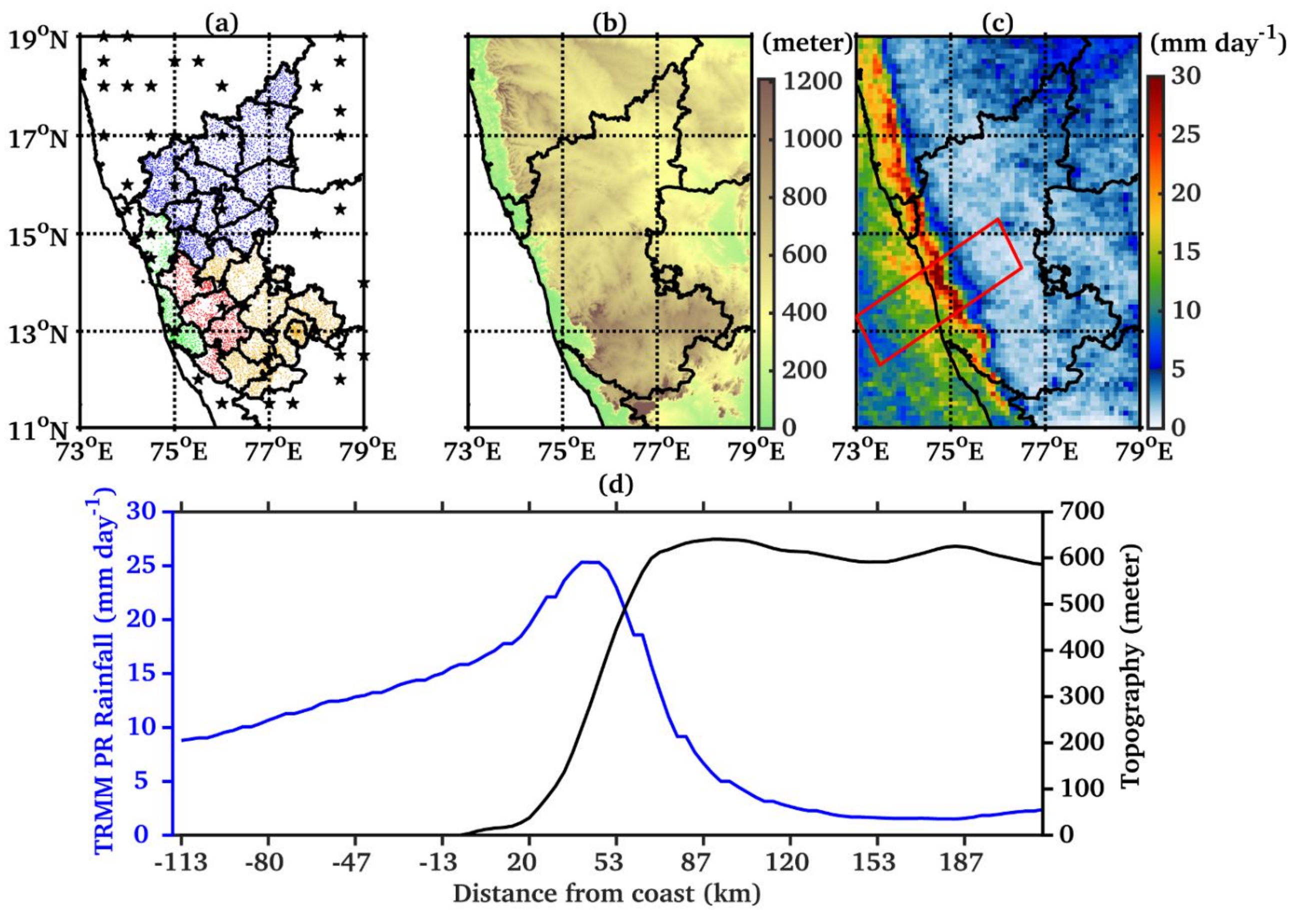

Fig. 1: Spatial distribution of (a) KSNDMC rain gauge network and NOAA/CPC rain gauge network over Karnataka, India. KSNDMC rain gauge stations over COASTAL (650), MALNAD (901), NIK (2737) and SIK (2214) regions are shown in green, red, blue and yellow dots, respectively. State boundaries of India and district boundaries of Karnataka state are shown as black lines. The black star shows location of NOAA/CPC gauges.(b) Spatial distribution of topography at 1 km spatial resolution, (c) mean JJAS rainfall at 0.1-degree spatial resolution from 13-years TRMM precipitation radar (PR) dataset and box covering the Western Ghats and oceanic regions, and (d) the cross-shore distribution of rainfall (blue line) and topography (black line) averaged across the red box (c) selected over the Western Ghats.

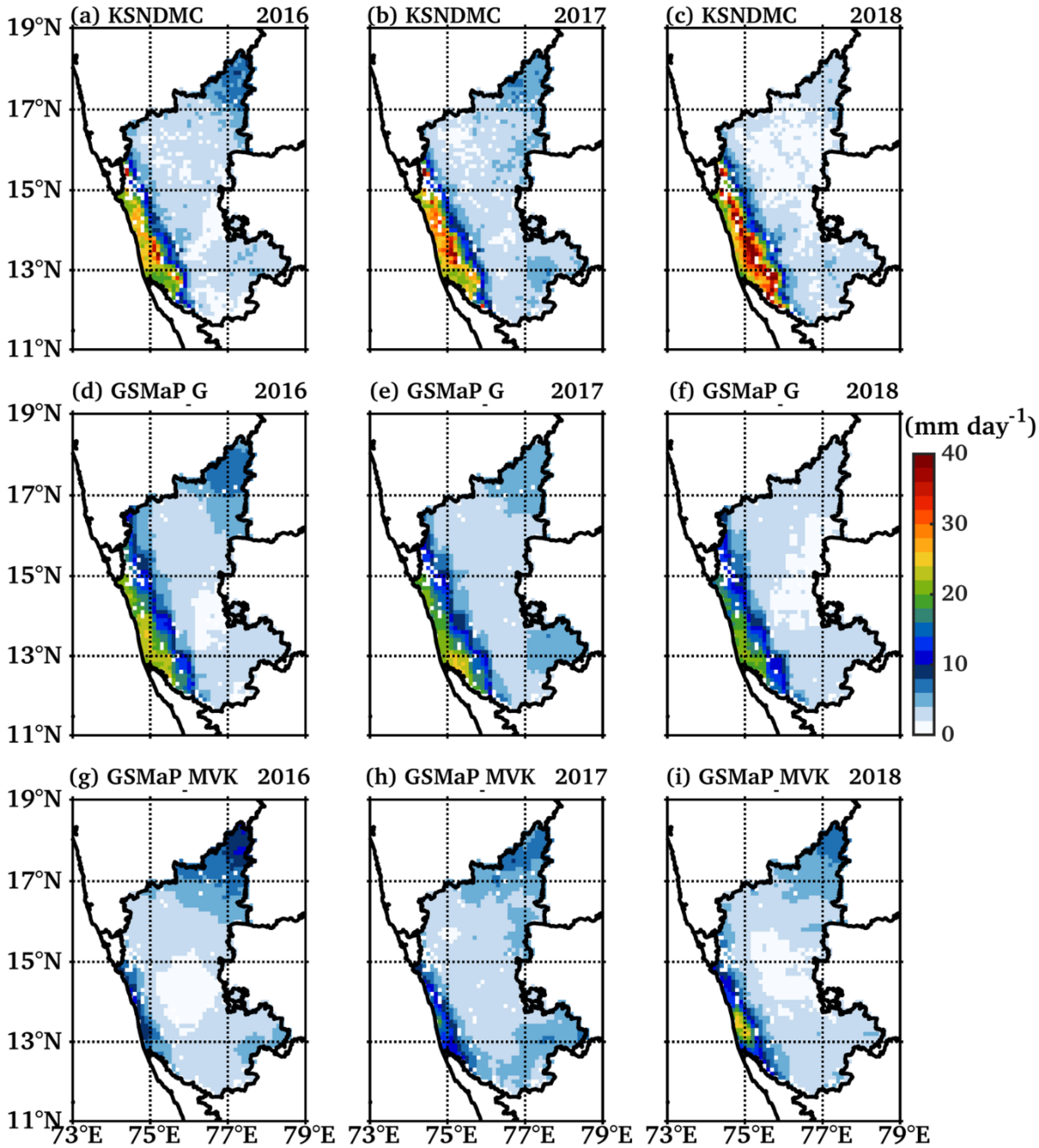

Fig.2: Spatial distribution of mean rainfall (mm day^{-1}) from KSNDMC rain gauges for (a) JJAS 2016, (b) JJAS 2017, (c) JJAS 2018;GSMaP_gauge (defined as GSMaP_G) rainfall for (d) JJAS 2016, (e) JJAS 2017, (f) JJAS 2018; and GSMaP_MVK rainfall for (g) JJAS 2016, (h) JJAS 2017, (i) JJAS 2018 over Karnataka, India.

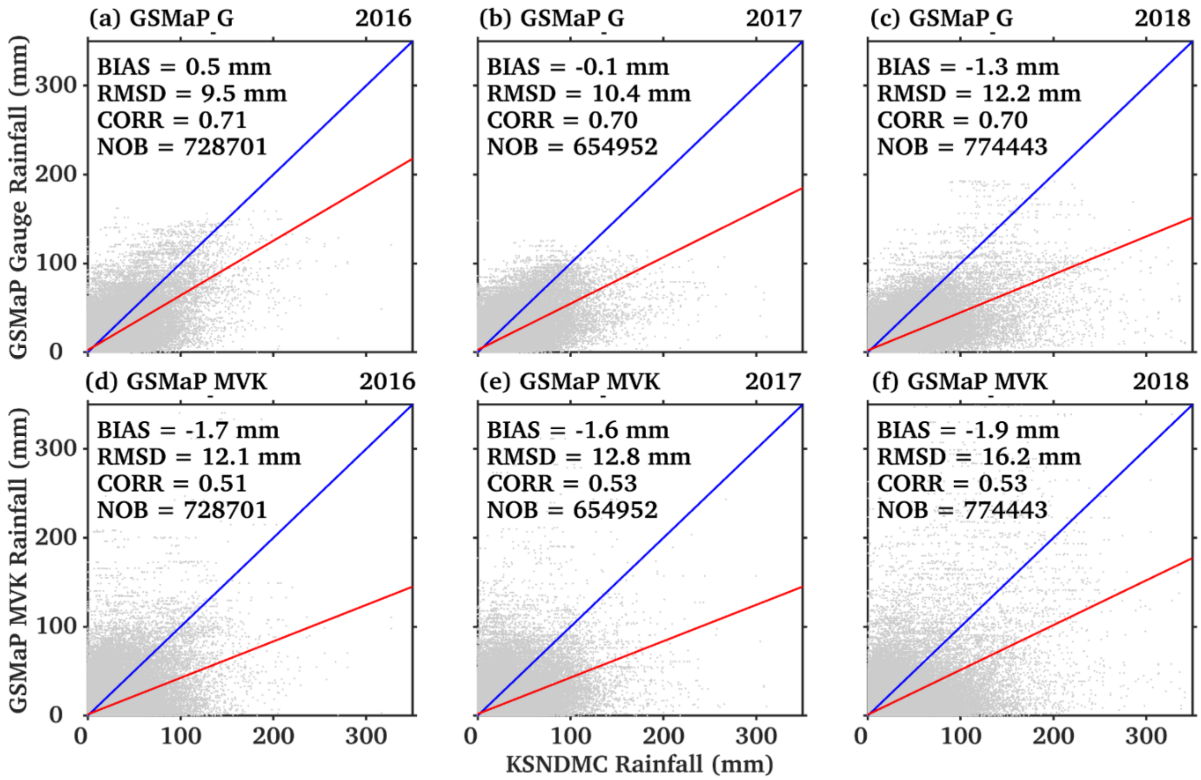

Fig.3: Scatter plot of GSMaP_Gauge daily rainfall against KSNDMC rain gauge observation during (a) JJAS 2016, (b) JJAS 2017, and (c) JJAS 2018. Scatter plot of GSMaP_MVK daily rainfall against KSNDMC rain gauge observation during (a) JJAS 2016, (b) JJAS 2017, and (c) JJAS 2018. The blue and red lines represent the 45° reference line and best fit line using least square method, respectively.

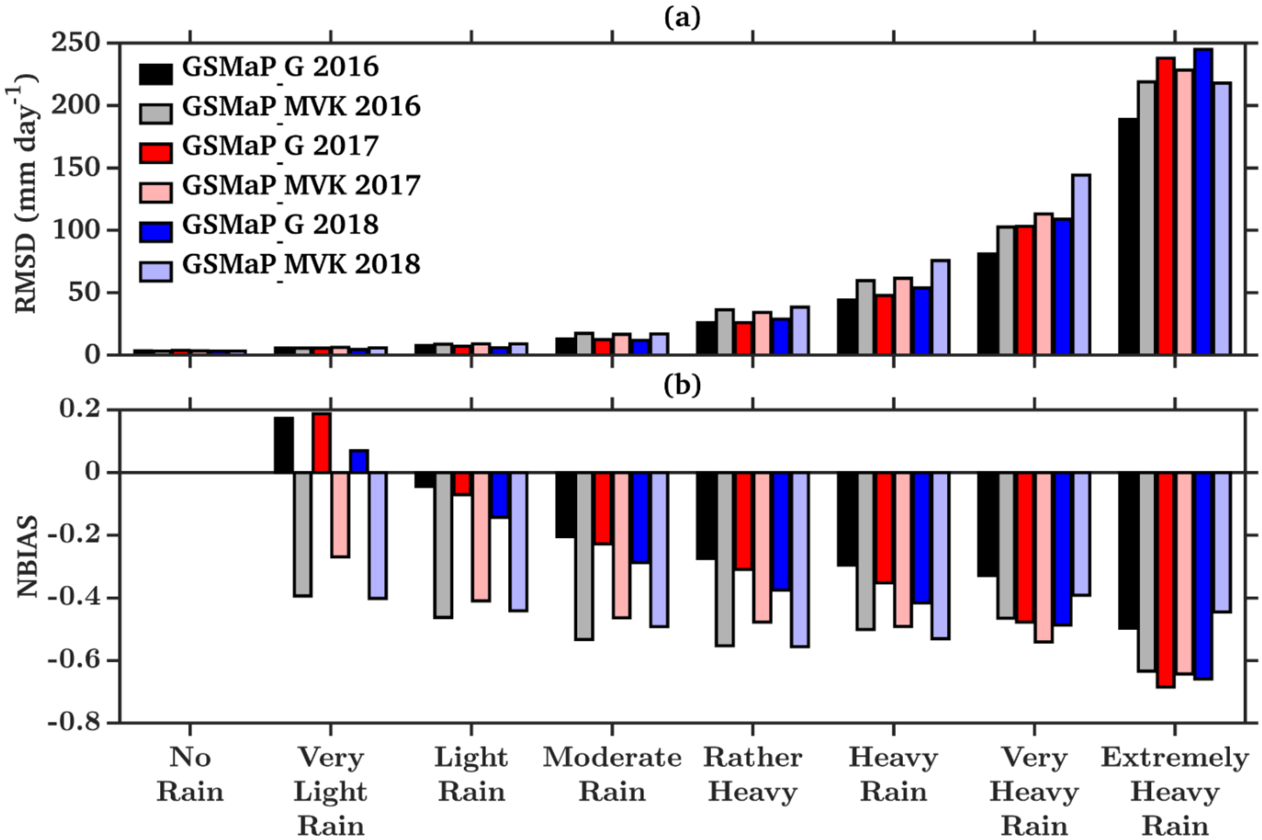

Fig.4: (a) RMSD and (b) NBIAS statistics of GSMaP_Gauge and GSMaP_MVK product for different IMD rainfall classifications as shown in Table 1.

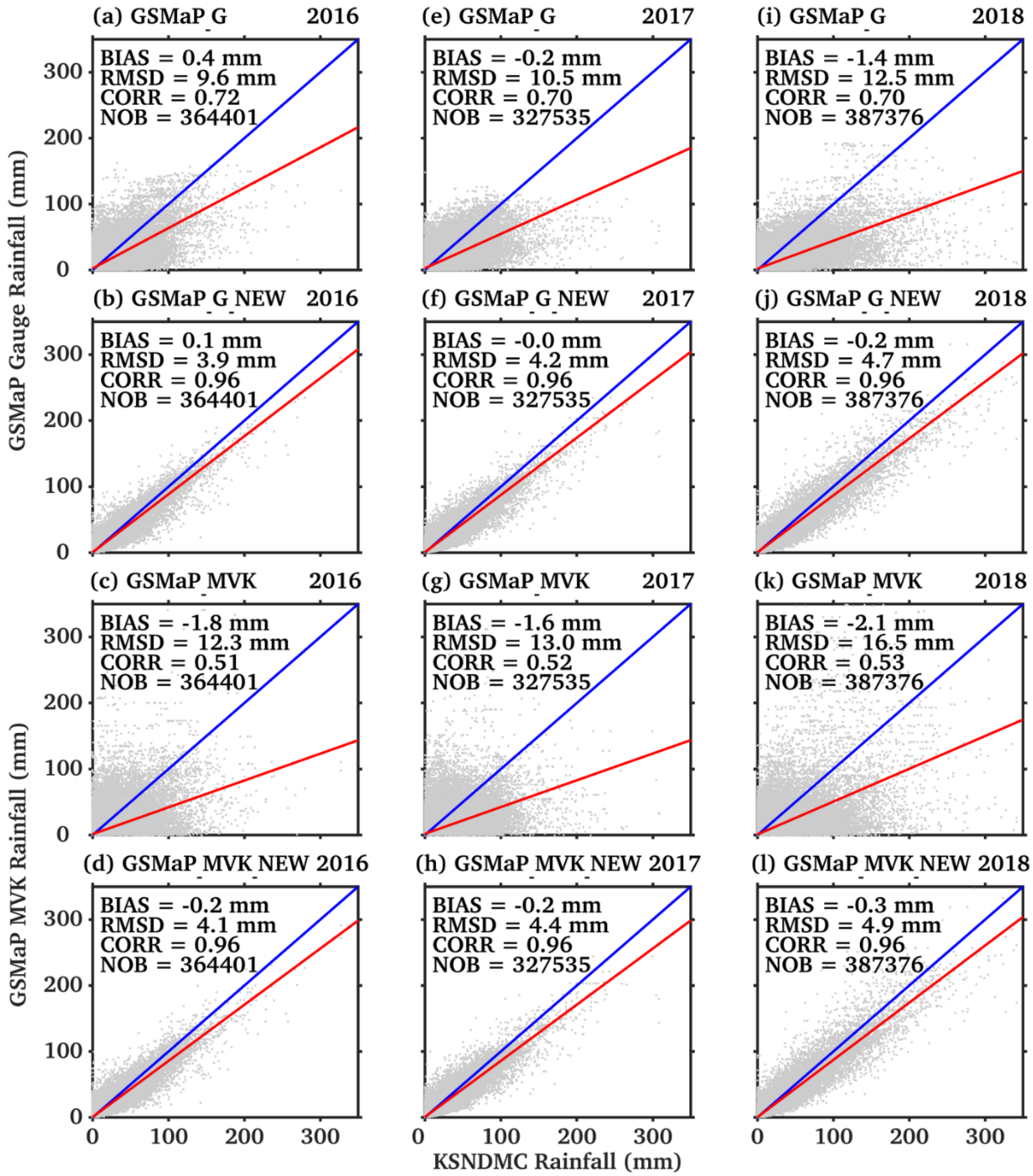

Fig.5: Scatter plot of GSMaP_Gauge daily rainfall during (a) JJAS 2016, (e) JJAS 2017, and (i) JJAS 2018; GSMaP_Gauge_NEW daily rainfall during (b) JJAS 2016, (f) JJAS 2017, and (j) JJAS 2018; GSMaP_MVK daily rainfall during (c) JJAS 2016, (g) JJAS 2017, and (k) JJAS 2018; GSMaP_MVK_NEW daily rainfall during (d) JJAS 2016, (h) JJAS 2017, and (l) JJAS 2018 against training gauges. Randomly selected 50 % rain gauges from the dense KSNDMC network are used as training gauges to prepare new rainfall products. The blue and red lines represent the 45° reference line and best fit line using least square method, respectively.

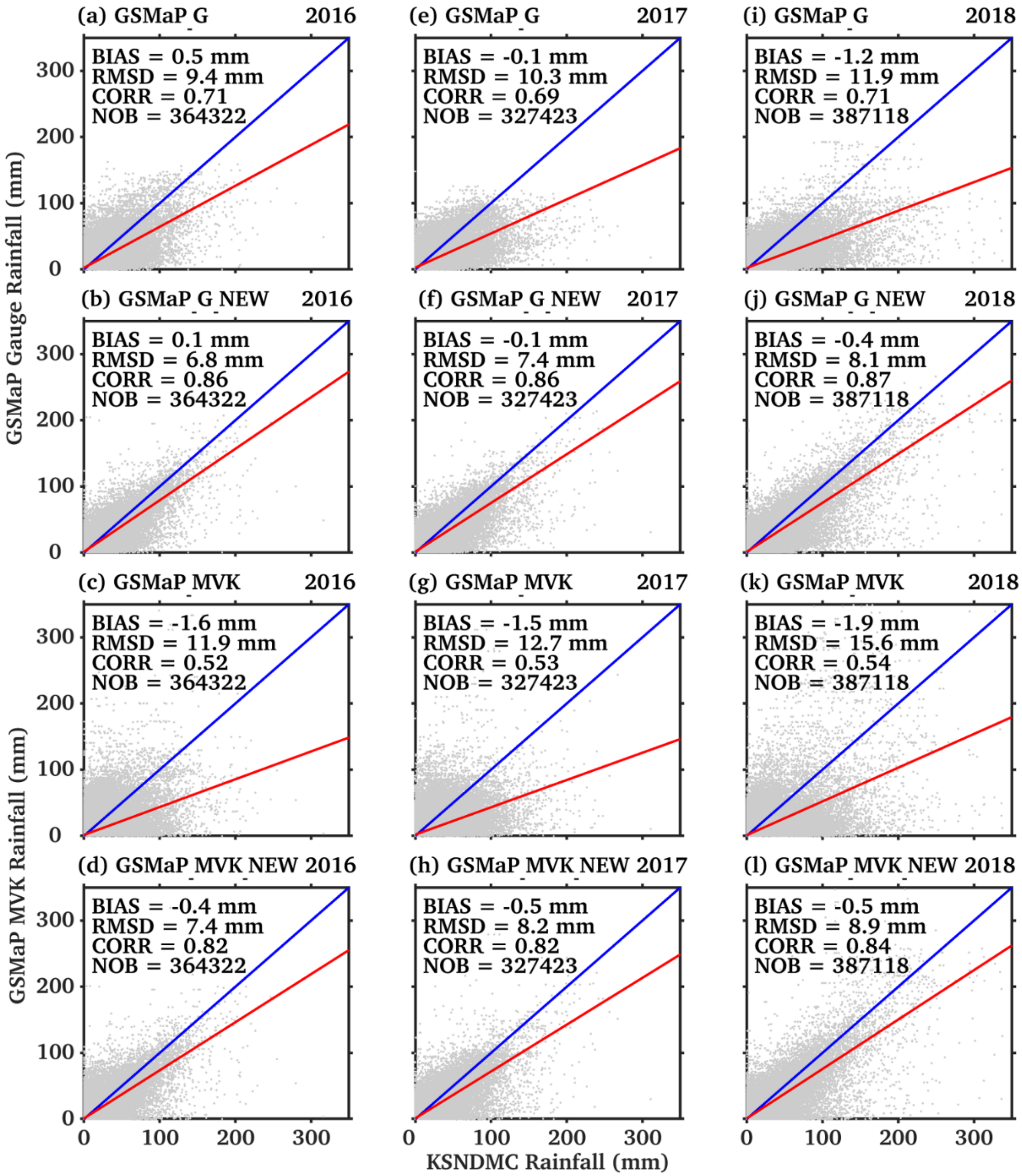

Fig.6: As in Fig. 5 but against verification gauges. The verification gauges are independent KSNDMC rain gauge observations.

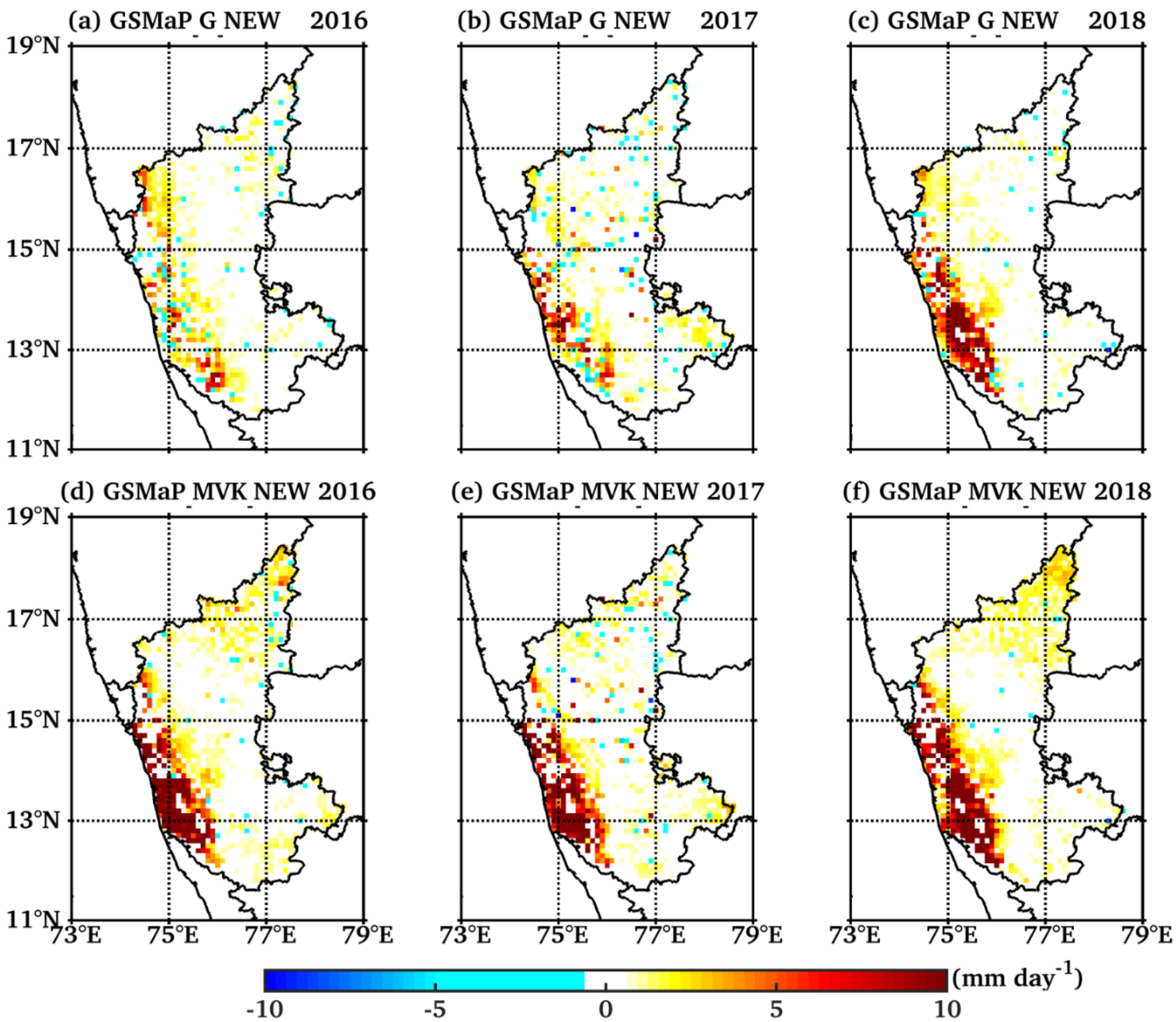

Fig.7: Spatial distribution of improvement parameter (*IP*) for GSMaP_Gauge_NEW during (a) JJAS 2016, (b) JJAS 2017, and (c) JJAS 2018; and GSMaP_MVK_NEW rainfall product during (d) JJAS2016, (e) JJAS2017, and (f) JJAS2018, respectively.

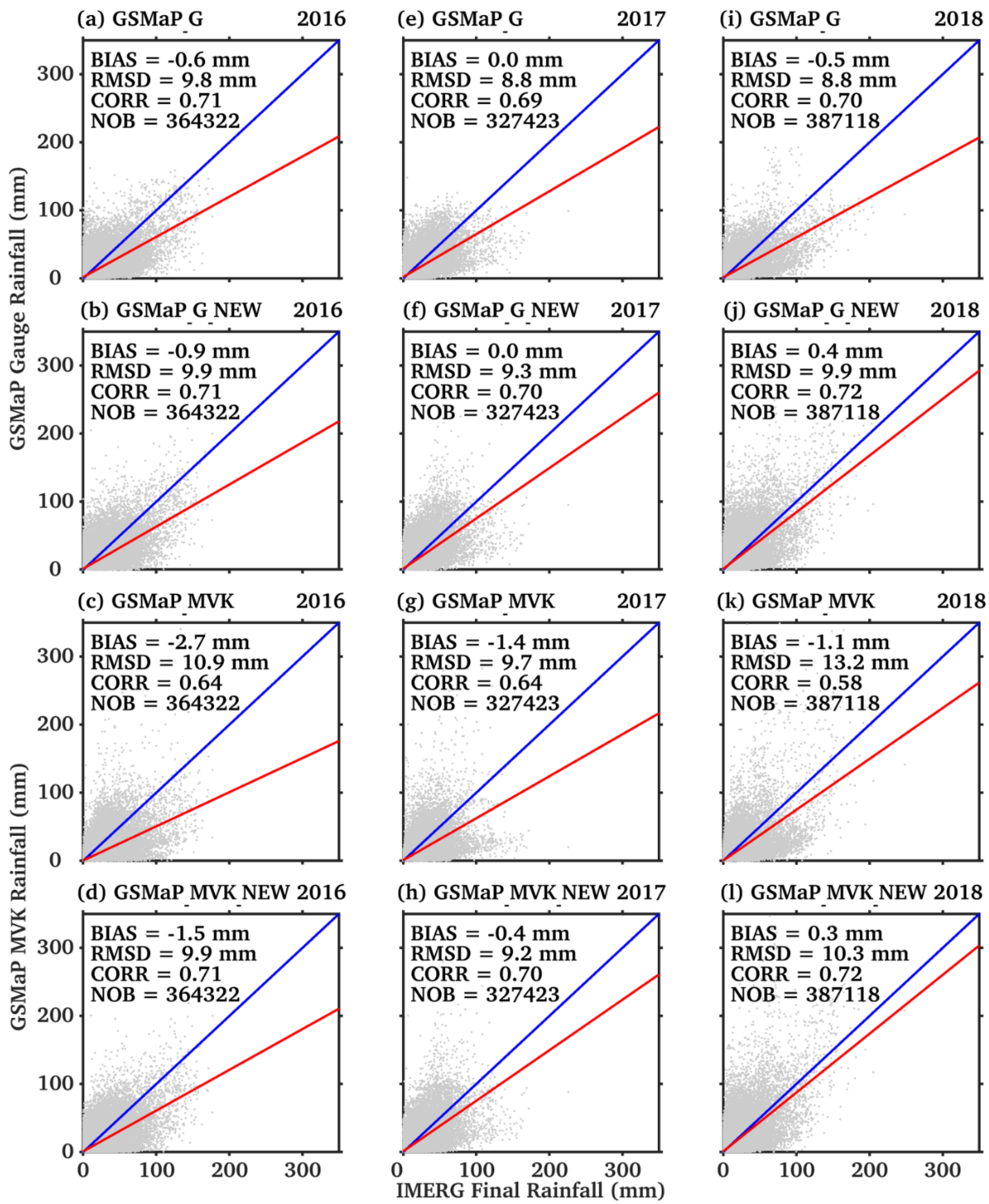

Fig.8: As in Fig. 5 but against IMERG final rainfall product.

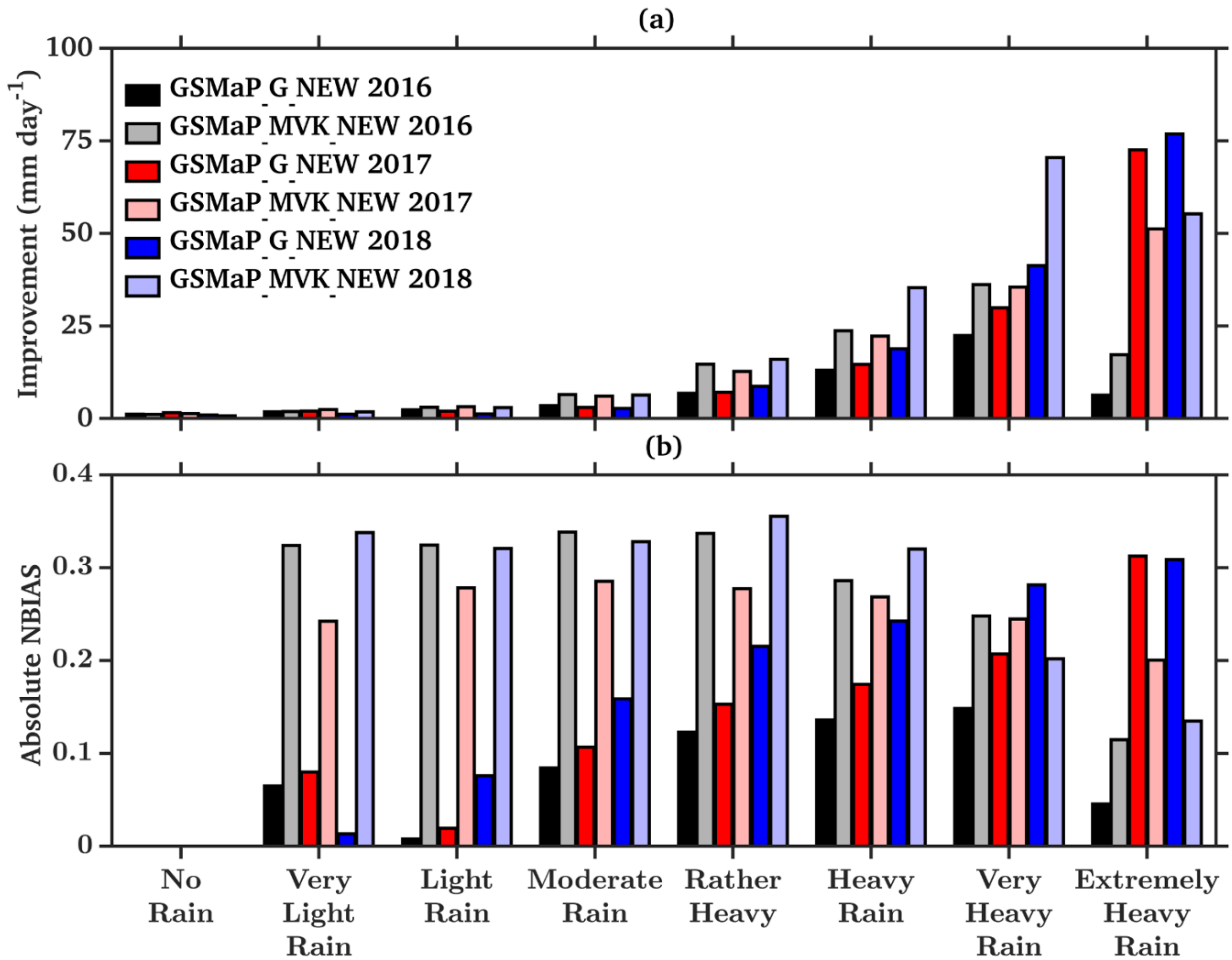

Fig.9: Error statistics of (a) Improvement parameter and (b) absolute NBIAS for GSMaP_Gauge_NEW (GSMaP_MVK_NEW) rainfall compared to GSMaP_Gauge (GSMaP_MVK) rainfall for different IMD classifications as shown in Table 1.

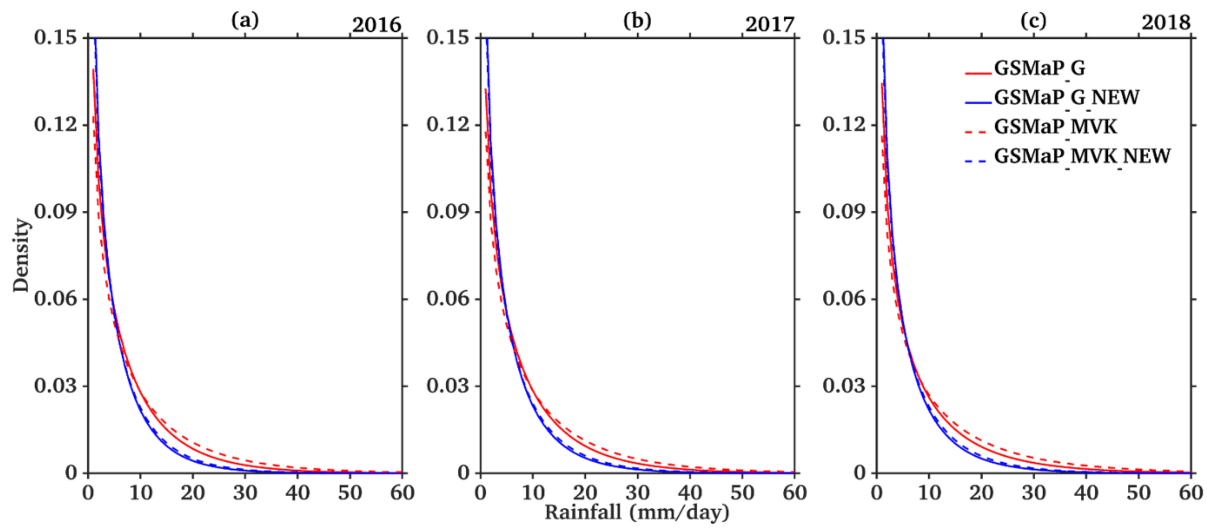

Fig. 10: Distribution of rainfall deviation (defined as GSMaP minus gauge) during (a) JJAS 2016, (b) JJAS 2017, and (c) JJAS 2018.

Table 1: IMD rainfall classification

Type	Amount of Rainfall
No rain	Rainfall amount realised in a day is 0.0 mm
Very light rain	Rainfall amount realised in a day is between 0.1 to 2.4 mm
Light rain	Rainfall amount realised in a day is between 2.5 to 7.5 mm
Moderate Rain	Rainfall amount realised in a day is between 7.6 to 35.5 mm
Rather Heavy	Rainfall amount realised in a day is between 35.6 to 64.4 mm
Heavy rain	Rainfall amount realised in a day is between 64.5 to 124.4 mm
Very Heavy rain	Rainfall amount realised in a day is between 124.5 to 244.4 mm
Extremely Heavy rain	Rainfall amount realised in a day is more than or equal to 244.5 mm

Table 2: Error statistics of GSMaP_Gauge and GSMaP_MVK rainfall against dense rain gauge networks over Karnataka, India

Region	Year	Satellite Rainfall	Data Points	BIAS (mm day^{-1})	NBIAS	RMSD (mm day^{-1})	Correlation
COASTAL	2016	GSMaP_Gauge	70789	-0.8	0.04	17.5	0.74
		GSMaP_MVK	70789	-14.6	0.03	25.5	0.58
	2017	GSMaP_Gauge	63556	-3.9	-0.07	19.9	0.71
		GSMaP_MVK	63556	-13.7	-0.65	34.9	0.37
	2018	GSMaP_Gauge	78411	-7.8	-0.45	24.7	0.74
		GSMaP_MVK	78411	-11.6	-0.52	38.3	0.58
MALNAD	2016	GSMaP_Gauge	105748	0.9	0.33	11.8	0.60
		GSMaP_MVK	105748	-4.4	0.28	13.3	0.46
	2017	GSMaP_Gauge	95184	-0.4	0.04	11.7	0.65
		GSMaP_MVK	95184	-4.5	-0.40	15.0	0.39
	2018	GSMaP_Gauge	108638	-5.2	-0.27	20.0	0.62
		GSMaP_MVK	108638	-7.8	-0.39	21.9	0.54
NIK	2016	GSMaP_Gauge	300645	0.9	0.43	8.0	0.63
		GSMaP_MVK	300645	0.4	0.43	9.7	0.55
	2017	GSMaP_Gauge	270460	0.4	0.40	7.8	0.57
		GSMaP_MVK	270460	0.3	0.11	8.8	0.57
	2018	GSMaP_Gauge	326989	0.5	0.19	6.5	0.50
		GSMaP_MVK	326989	0.8	0.10	8.7	0.49
SIK	2016	GSMaP_Gauge	256920	0.1	0.41	6.5	0.54
		GSMaP_MVK	256920	0.4	0.42	7.8	0.58
	2017	GSMaP_Gauge	230988	0.5	0.33	8.4	0.55
		GSMaP_MVK	230988	0.6	0.07	8.9	0.59
	2018	GSMaP_Gauge	266765	-0.1	0.23	6.4	0.54
		GSMaP_MVK	266765	0.1	0.07	7.5	0.50

Table 3: RMSD in daily GSMaP rainfall products using different assimilation methods and utilized rain gauge numbers (RG1, RG2, RG3).

Data	Training Rain Gauges	Operational (mm day^{-1})	Cressman Method (mm day^{-1})	Optimal Interpolation (mm day^{-1})	Hybrid method (mm day^{-1})
GSMaP_MVK	RG1	16.1	12.8	9.4	8.3
	RG2	16.1	14.6	11.2	9.2
	RG3	16.1	15.3	13.1	10.6
GSMaP_Gauge	RG1	12.1	10.7	8.4	7.6
	RG2	12.1	11.4	9.7	8.4
	RG3	12.1	11.8	10.7	9.1